Annual Report

Authors

Ron Adamson
Fremont, CA, USA

Kit Coleman
Ontario, Canada

Friedrich Garzarolli
Fürth, Germany

Albert Machiels
EPRI, CA, USA

Tahir Mahmood
Pleasanton, CA, USA

Charles Patterson
Clovis, CA, USA

Peter Rudling
ANT International, Mölnlycke, Sweden

A.N.T. INTERNATIONAL®

Advanced Nuclear Technology International
Analysvägen 5, SE-435 33 Mölnlycke
Sweden

info@antinternational.com
www.antinternational.com


Ecolabelled printed matter, 3041 0129

Disclaimer

The information presented in this report has been compiled and analysed by Advanced Nuclear Technology International Europe AB (ANT International®) and its subcontractors. ANT International has exercised due diligence in this work, but does not warrant the accuracy or completeness of the information. ANT International does not assume any responsibility for any consequences as a result of the use of the information for any party, except a warranty for reasonable technical skill, which is limited to the amount paid for this assignment by each ZIRAT/IZNA programme member.

Contents

1 Introduction (P. Rudling)

The objective of the Annual Review of ZIRconium Alloy Technology (ZIRAT) and Information on Zirconium Alloys (IZNA) is to review and evaluate the latest developments in ZIRAT as they apply to nuclear fuel design and performance.

The objective is met through a review and evaluation of the most recent data on zirconium alloys and to identify the most important new information and discuss its significance in relation to fuel performance now and in the future. Included in the review are topics on materials research and development, fabrication, component design, and in-reactor performance presented in conferences, journals and reports.

The primary issues addressed in the review and this report is zirconium alloy research and development, fabrication, component design, ex- and in-reactor performance including:

- Regulatory bodies and utility perspectives related to fuel performance issues, fuel vendor developments of new fuel design to meet the fuel performance issues.
- Fabrication and Quality Control (QC) of zirconium manufacturing, zirconium alloy systems.
- Mechanical properties and their test methods (that are not covered in any other section in the report).
- Dimensional stability (growth and creep).
- Primary coolant chemistry and its effect on zirconium alloy component performance.
- Corrosion and hydriding mechanisms and performance of commercial alloys.
- Cladding primary failures.
- Post-failure degradation of failed fuel.
- Cladding performance in postulated accidents (Loss of Coolant Accident (LOCA), Reactivity Initiated Accident (RIA)).
- Performance of accident tolerant fuel (ATF)
- Dry storage.
- Potential Burn-up (BU) limitations.
- Current uncertainties and issues needing solution are identified throughout the report.

Background data from prior periods have been included wherever needed. The data published in this Report is only from non-proprietary sources; however, their compilation, evaluations, and conclusions in the report are proprietary to ANT International and ZIRAT/IZNA members as noted on the title page.

The authors of the report are Mr. Friedrich Garzarolli, Dr. Ronald Adamson, Dr. Christopher Coleman, Dr. Tahir Mahmood, Dr. Albert Machiels (EPRI) and Mr. Peter Rudling, President of ANT International.

The work reported herein will be presented in four Seminars:

- February 13-15, 2017, Clearwater Beach, Fl., USA,
- March 6-8, 2017, Palma de Mallorca, Spain
- September, 2017 in China
- September, 2017 in Japan

The Term of ZIRAT21/IZNA16 started on February 1, 2016 and ends on March 31, 2017.

All literature that we refer to in this Report is available in the ANT International Literature Database (LDB). Please contact Ms. Angela Olpretean at angela.olpretean@antinternational.com for more information.

2 Burnup and fuel technology achievements (C. Patterson)

2.1 Introduction

The objective of this Section is to summarize the key performance issues that could affect fuel design, fabrication or operation of nuclear fuel in the near or longer terms. Topics covered relate primarily to the fuel itself. The latest zirconium alloy technology is covered in Section 3 and in related topical sections of the Annual Report. Similarly, information regarding accident tolerant fuel is given a later section of the Annual Report. The information sources reviewed, screened and evaluated include nearly all the related publications and technical meeting presentations of the past, approximately 18 months. This Section is intended to be a guide to current issues related to these topics and to provide an alert to items that could affect fuel related operations. The extensive volume of information involved limits the presentations to the most significant features and conclusions, and the reader is urged to refer to the referenced publications for more detail.

2.2 Trends in fuel and reactor operating conditions

2.2.1 General trends

The driving forces in the evolution of fuel technology and operating conditions are improved fuel reliability and economics while maintaining acceptable margins to operating and regulatory safety limits. These forces provide incentives for significant advances in materials technology, software for designing and predicting fuel performance, sophisticated instrumentation, modifications in water chemistry and methods for post-irradiation examinations. These forces are also causing shifts in the utilization of nuclear power in established and developing nuclear countries.

Advances in technology have increased the demands on fuel performance levels and put pressure on the regulatory bodies to license operations to increased burnup levels. The types of changes in LWR design and operating methods intended to achieve improved safety and economics have not changed in the past years and still include:

- Plant power uprates that range from 2 to ~20%,
- More aggressive fuel designs with a larger amount of fuel at or near the near-universal limit for civilian power reactors of 5% ^{235}U,
- Increased concentrations and more widespread use of burnable neutron absorbers,
- More aggressive fuel management practices, with increased power peaking factors and increased amounts of fuel operating closer to design limits,
- Annual fuel cycles extended to 18 and 24 months,
- Increased discharge burnups as high as 64 GWd/MT batch average exposures by higher enrichments, increased number of burnable absorbers in the assemblies and in PWRs higher lithium and boron levels or enriched boron in the coolant,
- Development of cladding and fuel assembly materials with increased resistance to corrosion, hydrogen pickup and radiation growth,
- Reduced activity transport by Zn injection into the coolant,
- Improved water chemistry controls and increased monitoring,
- Component life extension with hydrogen water chemistry (HWC), noble metal chemistry (NMC) and more extensively with on-line noble metal chemistry (OLNC) in BWRs.

Recent findings related to these issues are reviewed later in this section.

A combination of environmental, economic and sociopolitical issues are contributing to changes in the worldwide application of nuclear power. Through the fall of 2016, the International Atomic Energy Agency reported 450 nuclear power reactors with an “operational” status and a total installed

electrical production capability of 392.0 GWe[1], [IAEA, 2016]. The number of reactors with operational status and the associated generating capacities are shown by country in Figure 2-1. The number is changing due to the closure of plants because of a combination of age, economic, political and social considerations. The installed capacity of the U.S. France, Japan, China, Russia and the Republic of Korea accounts for approximately 2/3 of the total nuclear generating capability.

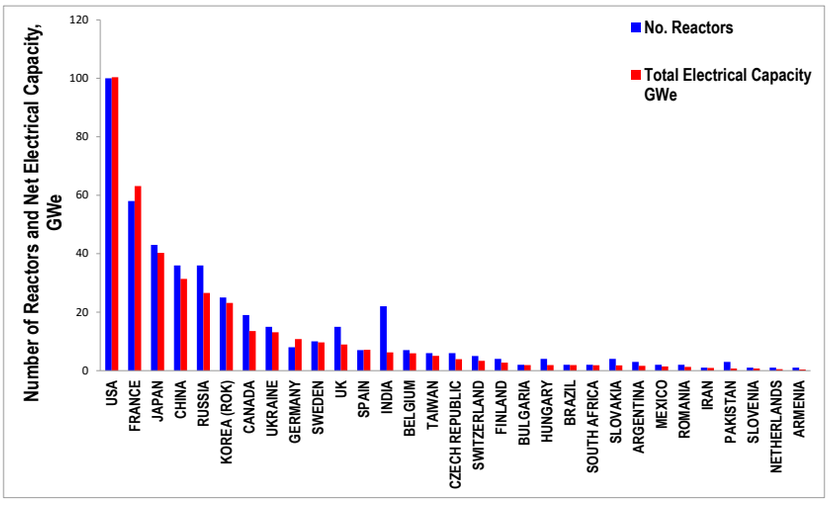

Figure 2-1: Electrical generating capabilities of nuclear reactors by country, after [IAEA, 2016].

The energy produced by the existing fleet of nuclear reactors constitutes about 10% of the worldwide energy production and about 23% in countries with nuclear power plants, [WNA, 2016] and [IAEA, 2016]. However, as shown in Figure 2-2, the relative role of nuclear power varies markedly among countries; e.g., 75% of electrical power from nuclear reactors in France and 0.5% in Japan. The large generating capacity and large nuclear fraction in France represents the historic policy of this country. The large capacity and the small production fraction in Japan represents the lingering effects of the 2011 Tohoku earthquake and tsunami; i.e., continued plant shutdowns with ongoing assessments of nuclear and plant safety by the utilities, regulators and politicians. The large generating capacity and small nuclear share in the U.S. and China reflects the reliance of these countries on alternate sources of energy – primarily fossil fuels.

[1] The Power Reactor Information System (PRIS) database of the IAEA includes experience of all nuclear countries. Information compiled in PRIS as of early fall-2016 is used as a primary source for information in this section. Although the database is updated at frequent intervals, information differs from regional databases and other periodic tabulations due to timing issues.

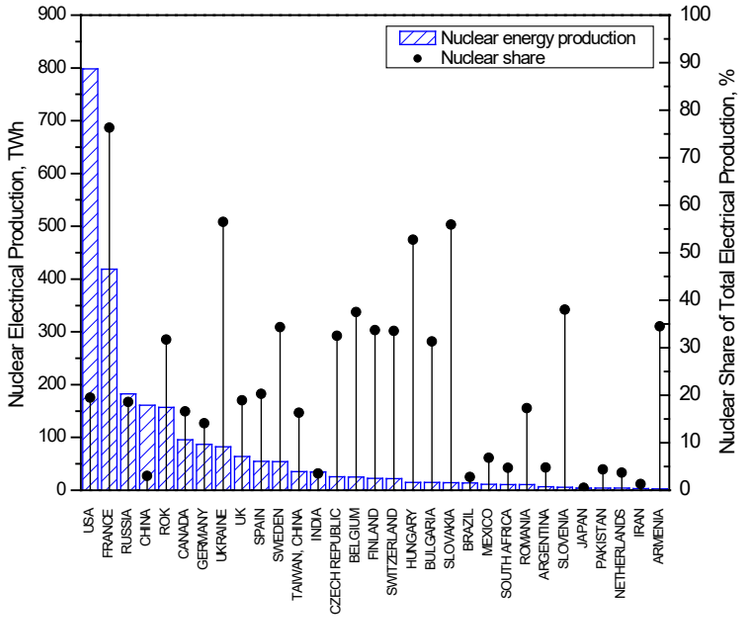

Figure 2-2: Electrical production by nuclear power plants and the share of nuclear to the total electrical production by country in 2016, after [IAEA, 2016].

Light water reactors continue to be most commonly used source of nuclear energy. As shown in Figure 2-3, PWRs and VVERs constitute the greatest number of reactors and the largest generating capacity; viz., 291 out of 450 reactors and ~70% of the operable nuclear generating capacity. This condition is expected to continue since 50 of the 60 reactors currently under construction are PWRs or VVERs, [IAEA, 2016].

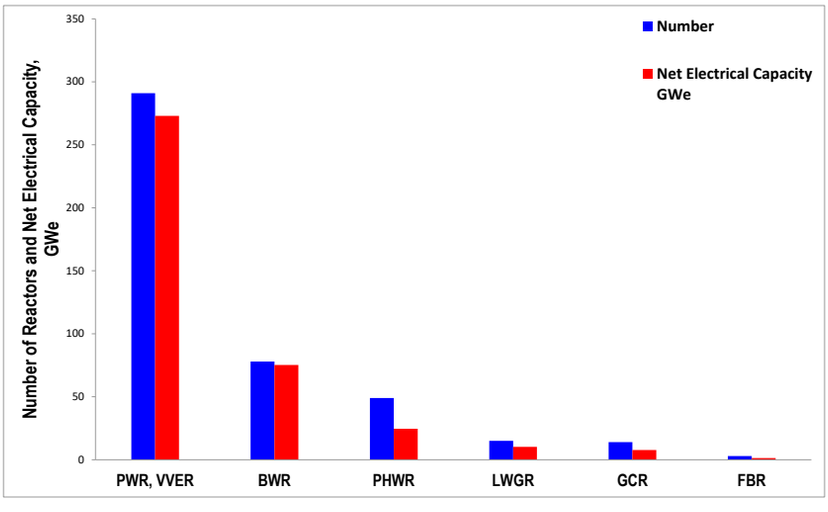

Figure 2-3: Number of operational nuclear reactors and net electrical generating capacity by reactor type, after [IAEA, 2016].

The relative contribution of nuclear power to the overall energy production in existing and new nuclear countries is likely to shift over time due to a combination of factors. As shown in Figure 2-4, a large number of new reactors are being constructed. Forty of the 65 reactors under construction at end of 2015 are being built in China, Russia, South Korea and India. Four reactors are being built in the US, 5 in Europe and 4 in the UAE. In addition reactors are being built in Argentina, Brazil, Belarus, Ukraine and Pakistan. At the same time, the age of the existing fleet of reactors in the established nuclear countries is approaching the point at which life extension or plant shutdown will

be needed (e.g., 40 yr in the US), Figure 2-5. The generating capacity shown in Figure 2-5 roughly corresponds to the number of plants. So, given the negative perception of nuclear power in many parts of Europe, Japan and the US, both the number of plants and the nuclear generation capabilities are expected to decrease in established nuclear countries and to increase in other countries over the next few decades.

A possible exception to the trend noted above is indicated by activity associated with small-to-medium sized, modular reactors (SMRs). These reactors are the subject of a large body of international work, with a few of the designs entering the prototype phase or being actively deployed in the case of barge-mounted reactors previously used in marine (ice breaker) applications.

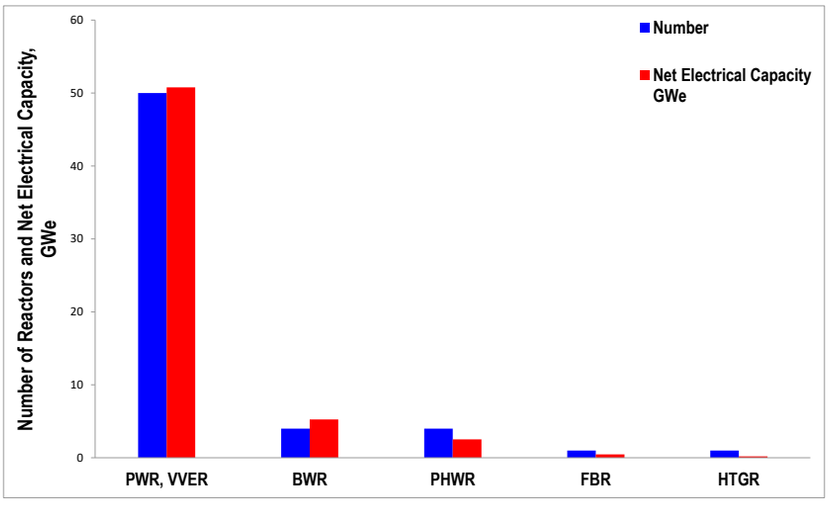

Figure 2-4: Reactors currently under construction by type, after [IAEA, 2016].

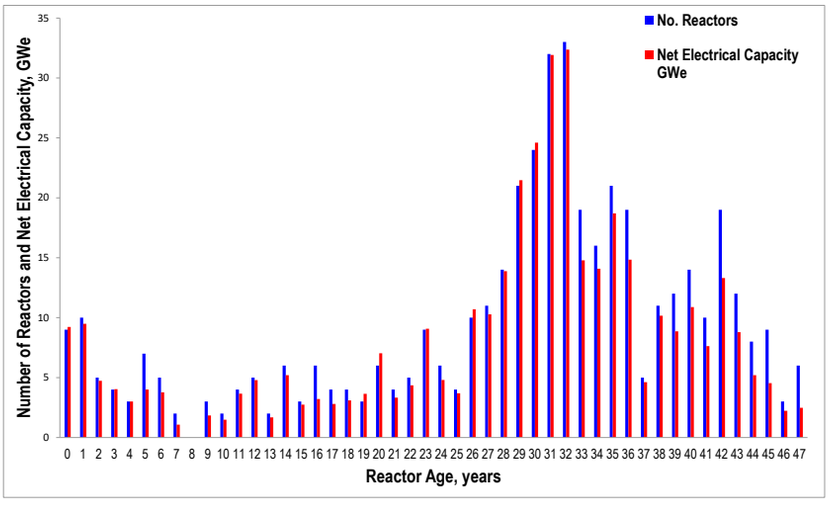

Figure 2-5: Age of operating reactors, after [IAEA, 2016].

2.2.2 Fuel cycles

2.2.2.1 Cycle length

The trend for increased fuel cycle lengths has come to a near “equilibrium” in the US with PWRs operating at an average of 500 effective full power days (EFPD) per cycle and BWRs an average of

620 EFPD per cycle, up to a maximum of about 680 days for PWRs and 720 days for BWRs.

Nearly all of the US BWRs are trending toward 24 month cycles except in an unusual move, Exelon changed the Clinton BWR NPP to a 12 month cycle. This change is reported to be in preparation for plant closure due to the economic effects of abundant, low-cost natural gas and subsidized, renewable sources. The older, lower power density PWRs have implemented the 24 month cycles, but fuel management limitations, specifically the reload batch sizes required, have limited implementation of 24 month cycles in the high power density plants. The economics of 24 month cycles tend to be plant specific since they depend on the balance of a variety of parameters unique to each plant. The potential economic gains for cycle extension have decreased in the US as the downtimes for reloading and maintenance procedures have been significantly reduced, thereby increasing the capacity factors.

Most countries outside the US have one, winter power peak annually compared to the two, winter and summer peaks in the US. This condition this has tended to keep plants outside of the US on annual cycles. Changes in load management, economics, maintenance practices and licensing procedures are influencing this condition; some countries, such as France, Belgium, Switzerland and Germany are applying both annual and 18 month cycles. The Russian fuel supplier TVEL has increased the fuel cycle length from 12 to 15 months in the 440 VVERs by increasing the enrichment from 4.2% to 4.7% in Russian, Finnish, Czech, Slovak and more recently in Hungarian plants.

2.2.2.2 Capacity factors

The capacity factors of US plants has been tracked for 3 year periods starting with 1975–1977 and extending through the 2012–2014 interval [Blake, 2015]. The number of plants covered since the 2009–2011 period has been reduced from 104 to 100, to account for plants that have been permanently shut down. The median capacity of the plants has been quite constant; i.e., close to 90%, ever since the period of 2000 to 2002. The mean capacity factors for the BWRs and PWRs have been nearly identical, with variations less than a 1% (Figure 2-6). The spread between the top and bottom quartile plants as a function of time is given in Figure 2-7 and shows that the top quartile has been above 92% consistently since the 1999–2001 period while the bottom quartile has improved and levelled off in the range of about 86 to 87%. It is of interest to note that the median capacity factor of multi-unit sites is slightly higher than for single unit sites in the 2012–2014 period. However, Blake observes that the effects of recent ownership changes on capacity factor data are unclear clear and that these relationships could be changing. The capacity factors for utilities that own more than one reactor site show a range of about 77 to 93%.

The latest information on capacity factors Nuclear Energy Institute[2] indicates the average capacity factor for all US reactors increased from 91.7% in 2014 to 92.5% in 2015.

[2] These data are accessible the NEI website at http://www.nei.org/Knowledge-Center/Nuclear-Statistics/US-Nuclear-Power-Plants/US-Nuclear-Capacity-Factors.

3 Microstructure and manufacturing

No new information has been added to this topic during the last year.

4 Mechanical properties (K. Coleman)

4.1 Introduction

In this section we will discuss strength, deformation and ductility. Strength is expressed in terms of properties like yield strength. Deformation and ductility are expressed in terms such as elongation at fracture or strain-to-some limit for a particular loading condition. Fracture resistance is a combination of strength and ductility that describes the conditions to initiate and grow cracks and estimate the point of crack instability. Each of these properties is affected by their alloy composition and fabrication route, and by the consequences of their residence in a nuclear reactor in hot water. Neutron irradiation changes the microstructure thereby affecting the mechanical properties. For example, <a>-dislocation loops strengthen zirconium but when annihilated by strain, ductility and fracture toughness are reduced. Corrosion adds an oxide layer and produces hydrogen, some of which is picked-up by the components. Hydrogen is important because it forms hydrides that can lead to embrittlement. During fission, extra gasses are formed adding to the internal pressure inside a fuel rod that is important during LOCA and spent fuel storage. Vibrations between touching surfaces can produce wear and fretting that may be so severe that protective membranes are breached. All these changes have to be accommodated to assure that components function as designed. Often each of the properties is studied separately but provide input to computer codes to explain experiments and guide assessments for fuel performance. Contributions to some of these items were made during the year with a notable emphasis on hydrogen effects. Examples are summarised in the following sections.

4.2 Surface damage

One of the fuel development challenges is to produce fuel that does not leak, especially during reactor operation. Historically, leakage has been caused by problems during fabrication, handling, pellet-clad interactions especially linked with fission products, and wear, either from debris fretting or fretting of cladding in spacer grids. The first three causes are under control but wear problems, although much improved, still exist. For example, in the US reactors using AREVA's fuel, 41 failed fuel rods were found in 2010 but in 2015 no fuel rods failed [Mazurkiewicz et al., 2016]. Vigilance is still required. In BWRs debris can come in different forms; from disintegration of a component or debris movement into the reactor heat transport system from locations of plant maintenance into the reactor core. The debris can become trapped between the fuel rod and spacer where it can vibrate in the fluid flow causing wear penetration of the cladding. Figure 4-1 shows a typical debris failure in a BWR fuel rod.

Figure 4-1: Cladding penetrated by debris [Mazurkiewicz et al., 2016].

Protection is provided by debris filters, called FUELGUARD™, that have been in development since the 1990s and are now on their third generation. These filters are operating in both BWRs and PWRs. They are reported to be very effective.

Also in BWRs, a few rods failed by pellet-clad-interaction (PCI) caused by missing some of the fuel pellet surface (MPS). This feature can result in a stress concentration, either over the missing fuel chip or by bending, and lead to cracking, Figure 4-2. MPS represents a quality control problem. This problem was eliminated by first altering power manoeuvring during operation then, once MPS was

identified as a cause, changing the fuel pellet design to include a chamfer and inspecting every pellet from two sides. Once these design and fabrication modifications were implemented, no PCI failures have been observed since 2007.

Although fuel has not failed by PCI in the US in the past 10 years, increasing PCI margins during reactor operations are still being developed. Tracking the thermal-mechanical condition of the fuel online has improved the efficiency of fuel manoeuvring. Protection from PCI by reducing the stress in the cladding is also obtained by using Cr_2O_3-doped fuel [Cole et al., 2012].

Figure 4-2: Example of PCI failure at MPS [Mazurkiewicz et al., 2016].

Grid-to-Rod Fretting (GTRF) has been the dominant failure mechanism in PWRs, Figure 4-3. It is caused by vibration of a fuel rod in contact with spacer grids driven by cross-flow in the heat-transport water. The amount of cross-flow depends on the reactor design.

Figure 4-3: Grid-to-Rod Fretting wear indication in PWR fuel cladding after interaction with spacer [Mazurkiewicz et al., 2016].

This fretting wear has been much reduced, even eliminated, by the development of a High Mechanical Performance (HMP™) lower grid made from Alloy 718 and a High Thermal Performance (HTP) grid configuration, Figure 4-4. These designs provide several line contacts between the grid and the fuel rod and helps to damp out vibration caused by water flow. The low in-reactor deformation of the grid supports the grid sufficiently to prevent rod rotation.

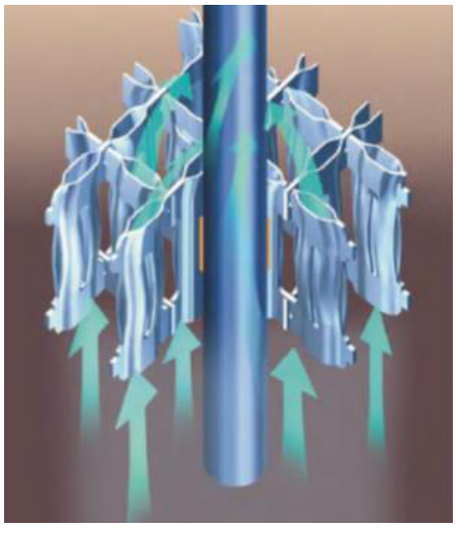

Figure 4-4: HTP™ grid configuration [Mazurkiewicz et al., 2016].

Some GNF2 fuel has failed in BWRs by debris damage, but only in pumped-forward drain plants (that have a history of this type of problem) and some plants that have had recurrent debris failures [Schneider et al., 2016]. A later design, GNF3, [Cantonwine et al., 2016] should much reduce problems with leakers and control blade interference. Debris wear is being reduced by spacer designs with low debris entrapment and improved debris capture in the Defender™ filter. GNF3 is being delivered with the fuel bundle and channel together in a fully assembled configuration, which eliminates the need to insert fuel channels over the bundles at the reactor site. To enable this innovation, the GNF3 spacer was designed to withstand the potential high-cycle and low-cycle fatigue conditions that can occur during shipping. Channel distortion from fluence gradient-induced bow and shadow corrosion-induced bow, causing channel – control blade interference, has been minimised by making the channels out of the alloy called NSF (Zr-1%Nb-1%Sn-0.4%Fe). This alloy is resistant to breakaway irradiation growth that causes fluence bow [Cantonwine et al, 2016]; in comparative tests the bow with NSF channels was one third that of Zircaloy-2 channels. Similar comparative tests under conditions susceptible to shadow bow showed that the amount of bowing of NSF was about one-fifth that of Zircaloy-2. Although the amount of corrosion was slightly greater in NSF than in Zircaloy-2 under BWR conditions, the hydrogen pick-up in NSF was 25% of that in Zircaloy-2.

4.3 Hydrogen effects.

Several basic properties of hydrogen in zirconium are relevant for evaluating components:

- The solubility limit for hydrogen in the α-phase of zirconium alloys is very low. With dynamic measurements, hydrides precipitate at a temperature, called TSSP, about 50 to 60°C lower than the temperature at which they completely dissolve, called TSSD, Figure 4-5 [based on Anonymous, 2013a]. Only one equilibrium solubility limit is possible so either TSSP (the Terminal Solid Solubility for Precipitation) or TSSD (the Terminal Solid Solubility for Dissolution) or neither are the equilibrium solubility limit. For practical purposes TSSP indicates the start of hydride precipitation and TSSD indicates when all the hydrogen has gone into solution.
- In practice, either δ-hydrides or γ-hydrides precipitate. δ-hydrides have a cubic crystal structure and a composition between about $ZrH_{1.4}$ and $ZrH_{1.6}$. They form in plates or groups of platelets that appear in light microscopy as line traces. γ hydrides have a tetragonal crystal structure and a composition of ZrH. They tend to form as needles. According to the Phase Rule only one hydride can be in equilibrium with the Zr matrix so most observations of mixed hydrides do not represent equilibrium.

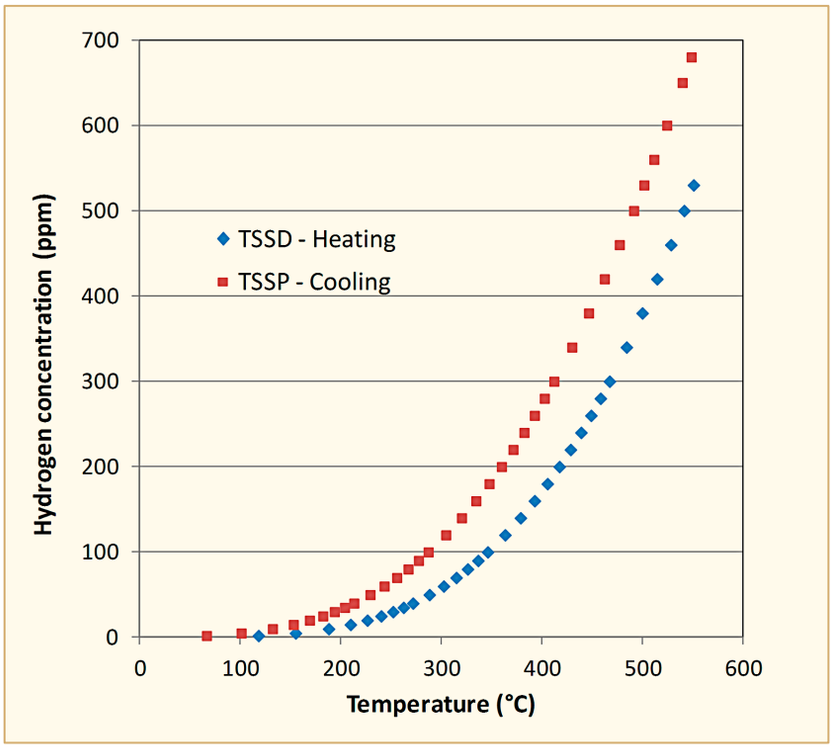

Figure 4-5: Typical temperature dependence, up to the eutectoid temperature, of values of hydrogen concentration in solution in zirconium when hydrides dissolve on heating and precipitate on cooling; this example is for Zr-2.5Nb, based on [Anonymous, 2013a].

- Hydrogen in solution generally expands the zirconium crystal lattice while hydrides tend to expand the zirconium lattice locally.
- Hydrogen diffuses in zirconium very quickly; at typical reactor temperatures hydrogen atoms diffuse about 10^{12} times faster than Zr atoms; for modelling the Zr atoms can be considered as stationary.
- Hydrides are brittle with a K_{IC} of about 1 to 3 MPa√m [Simpson and Cann, 1979]. It is this property that represents a possible danger for cracking of a component.

4.3.1 Dimensional change

Hydrogen in solution can contribute to dimensional changes through lattice expansion and interactions with dislocations while hydrides can reduce creep rates in unirradiated materials. The important question to answer is whether there are hydrogen effects on dimensions during irradiation. Stress-relieved Zirlo and recrystallized Zr-1Nb tubes containing a range of hydrogen concentrations that ensured the presence of hydrides were pressurised to various values then irradiated at between 301 to 312°C within spacer rods for up to four reactor cycles and their lengths and diameters were measured at intervals [Foster et al., 2016]. Irradiation growth is the dominating strain component in the axial direction. A small increase in axial growth due to hydrogen was observed in Zirlo, Figure 4-6, whereas in Zr-1Nb the contribution was also small but negative. Irradiation creep is the dominating strain component in the transverse direction. Within the scatter of the data, the diametral creep was unaffected by either the small amount of hydrogen in solution or the presence of hydrides, Figure 4-7. A small amount of growth was also observed in the transverse direction. Thus one can conclude that a pick-up of up to 720 ppm hydrogen has little effect on in-reactor deformation.

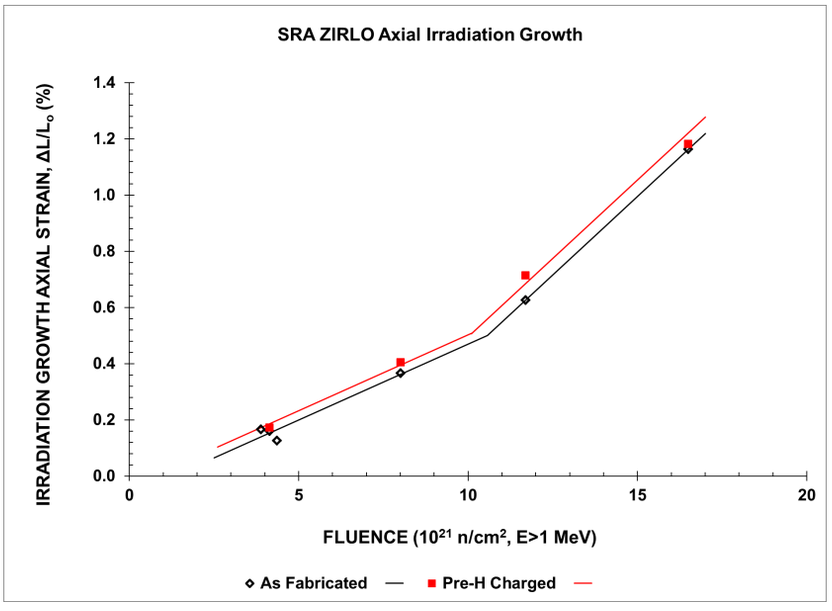

Figure 4-6: Fluence dependence of irradiation growth in the axial direction of SRA Zirlo tubes irradiated between 301 to 312°C showing small effect of hydrogen concentration [Foster, 2016].

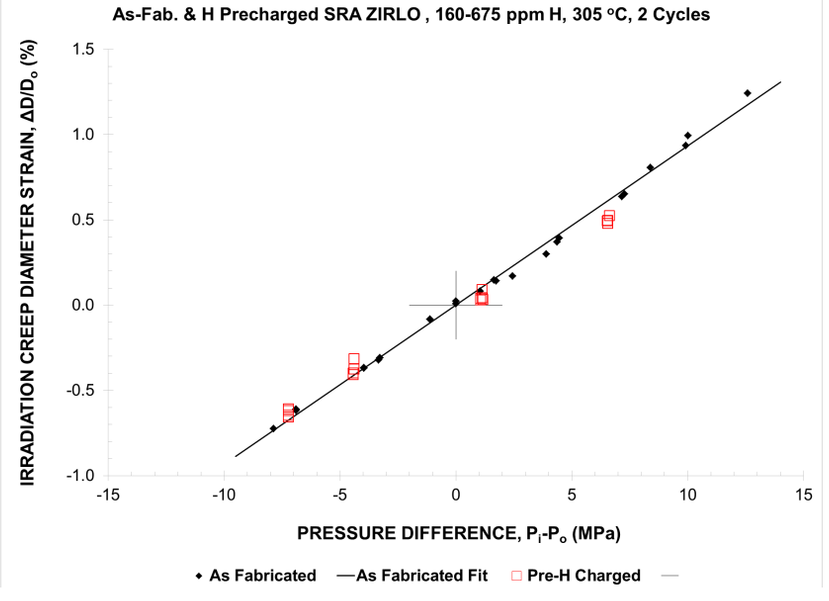

Figure 4-7: Effect of pressure on in-reactor diametral creep of SRA Zirlo at 305°C showing little effect of hydrogen concentration up to 675 ppm [Foster, 2016].

4.3.2 Hydride orientation

Hydrides with their plate normals parallel to an applied stress may lead to severe loss in ductility. In a tube, hydrides may be oriented with their normal in the hoop direction – these hydrides provide a trace in the radial direction, as observed by light metallography, and are called radial hydrides. Current tube components are fabricated so hydrides are oriented with their normal in the radial direction - these hydrides form with their trace in the circumferential direction, and are called circumferential hydrides. Several methods are used to describe radial hydrides. Typically for tubes, hydride orientation is often quoted as F_n, the fraction of the number or length of hydrides with trace angle to a reference direction in a plane that is in the range x to 90°, where x is usually > 45°; values will range from 0.0 to 1.0 [Anonymous, 2013b]. The appeal of such methods is that the trace of the edge of the

hydride is easily observed by light metallography. After a thermal cycle that dissolves hydrides, if the hoop stress is greater than a threshold stress, σ_R, on cooling to a low temperature where hydrides precipitate, radial rather than circumferential hydrides may form. The radial hydrides are the result of stress reorientation. Experiments are done to evaluate the stress and temperature history required to nucleate radial hydrides and to assess their effect on ductility to help answer questions on the behaviour of cladding during normal operation and during dry storage. In material with some cold-work and elongated grains, σ_R is often found to be 60 to 100 MPa. In annealed materials with equiaxed grains, hydrides may precipitate with a radial orientation in grain boundaries with no stress so the evaluation needs to take the initial orientation into account.

The potential for radial hydrides to reduce the tolerance for handling accidents as part of spent fuel storage has been evaluated in stress-relieved Zirlo™ [Kesterson et al., 2016]. Diameter crush (or pinch) loading was represented by ring-compression tests (RCT) while three-point bend tests (TPB) were used to represent fuel rod bending. High purity hydrogen was charged up to 800 wt.ppm in sections of tubes at 400°C that were then pressurized in argon to hoop stresses of 90, 130 and 170 MPa and cooled at 5 °C/h from 400°C to 200°C under pressure. With this maximum temperature, if the material contained more than 200 wt.ppm, which is the expected solubility limit, then the microstructure would be expected to consist of a mixture of radial and circumferential hydrides. Often radial hydride growth terminated when intersecting existing circumferential hydrides, Figure 4-8. No radial hydrides were observed with a hoop stress of 90 MPa.

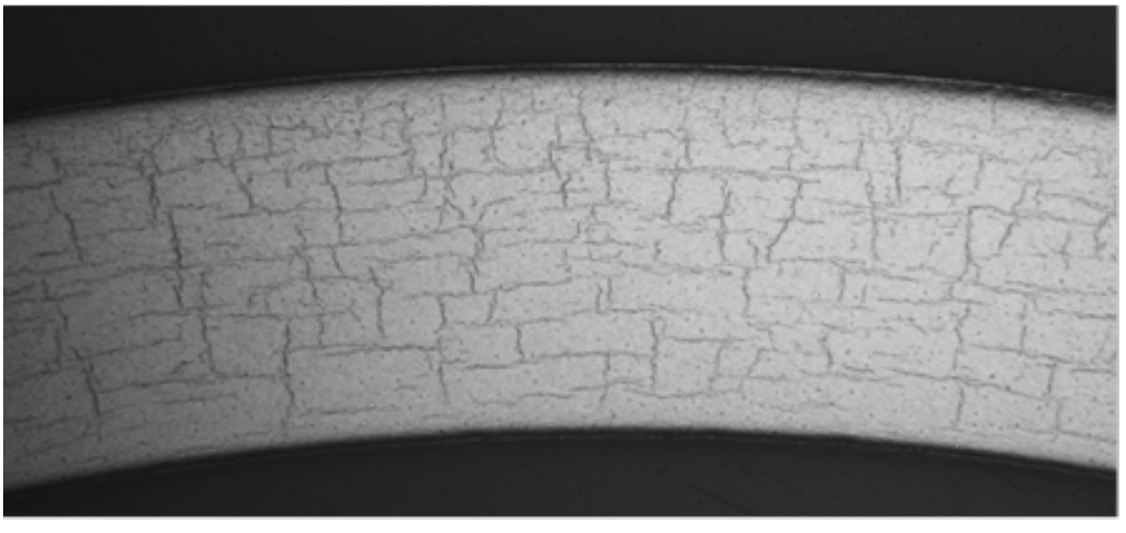

Figure 4-8: Radial hydrides in stress-relieved Zirlo fuel cladding containing 200 ppm hydrogen cooled from 400°C under a hoop stress of 170 MPa; the tube wall thickness was 0.57 mm. [Kesterson et al., 2016].

The test set-up for RCT is depicted in Figure 4-9 showing how the 8 mm long specimen was compressed at a cross-head speed of 5 mm/s. Tests were done between room temperature and 200°C to simulate interim long term storage. Typical load-displacement curves are shown in Figure 4-10. During plastic yielding abrupt load drops were observed that were associated with cracking; the plastic displacement at the initial load drop was used to determine failure strain and lead to a brittle-to-ductile transition temperature, Figure 4-11. This temperature was controlled by the relative amounts of radial hydrides. Specimens containing 100 and 200 wt.ppm hydrogen had a high fraction of radial hydrides and the highest transition temperature whereas specimens with 400 and 800 wt. ppm hydrogen had a low fraction of radial hydrides and the remaining circumferential hydrides did not contribute to a decrease in ductility. Despite these low strain failures at low temperatures, during pinching the fuel pellets restrict diametral displacement to pessimistic value of 0.15 mm before contact. This value is over three times smaller than the lowest displacement before failure in the RCT.

5 Dimensional stability/ Meetings review (R. Adamson)

5.1 Dimensional stability will be reviewed in full in ZIRAT22

This due to the fact that most final papers are not yet available.

5.2 Overall Review of Two International Meetings

5.2.1 18th International Symposium Meetings on Zirconium in the Nuclear Industry, May 2016

This prestigious ASTM meeting was held in Hilton Head, South Carolina.

Administrative highlights include:

- Chairman, Bob Comstock, Westinghouse. Editorial Chairman, Arthur Motta, Penn State
- Over 100 technical abstracts submitted
- 41 papers accepted for oral presentation
- 20 papers accepted for poster presentation
- 10 countries represented
- 137 registrants, including 20 students
- 16 student authors or co-authors, which is believed to be a record
- 3 Kroll Medal awards and papers
    - Drs. RA. Murgatroyd and A. Rogerson for work on irradiation growth of zirconium alloys
    - Prof. A.T. Motta for wide-ranging work on mechanisms involved in zirconium alloy component performance.
    - Dr. T. Fuketa for understanding of component performance during accident conditions.
- John Schemel Award for Best Paper from 17th International Symposium: "Effect of Hydrogen on Dimensional Changes of Zirconium and the Influence of Alloying Elements: First-Principles and Classical Simulations of Point Defects, Dislocation Loops and Hydrides," M. Christensen, W. Wolf, C. Freeman, E. Wimmer, R.B. Adamson, L. Hallstadius, P. Cantonwine and E.V. Mader
- Sessions:
    - Processing and Mechanical Behavior (6 papers)
    - Mechanisms of Corrosion and Hydrogen Pickup (6 papers)
    - Irradiation Effects on Oxide Microstructure (6 papers)
    - Irradiation Effects and Growth (6 papers)
    - In-Reactor Performance (7 papers)
    - High Temperature Transients (6 papers)
    - Hydrogen Effects and Dry Storage (5 papers)

5.2.1.1 Technical highlights in dimensional stability and microstructure areas include:

With the in-flux of university students and national labs into the nuclear materials field, many "new" investigation techniques are being introduced. Some of these techniques are covered in the ZIRAT20STR "Microstructure of Zirconium Alloys and Effects on Performance," while others will be covered in detail in a later ZIRAT STR. A particularly interesting example is the paper of **Hu et al.**, who used many techniques to study SPPs and microstructure of Zircaloy-4. While the new techniques do add new details and insight to various material performances, we must be careful not to jump to conclusions until the new data are assimilated into the existing databases.

Two papers present micro-computational-models for the mechanism of irradiation growth **[Christensen et al. and Golubov et al.]**. The first paper is an extension of previous work (Best Paper Award above) in which quantum mechanics and molecular dynamics are applied to the motion and interaction of defects believed to cause growth. This work is on the verge of explaining many experimental observations, such as the influence of Nb or lowering growth. The second paper (also an extension of previous work) presents a model which purports to explain the shape of the growth curve in Zircaloys and the co-existence of vacancy and interstitial loops. The two papers do not agree on some basic radiation-damage geometry and diffusion characteristics, and a meeting-of-the-minds in this area would be useful.

Yagnik et al. present extensive new data on effects of alloying elements and hydrogen on irradiation growth of a wide range of Zr-alloys. Irradiations were conducted in the BOR 60 reactor at 320ºC. Results include: Fe additions lower growth; Nb additions lower growth; H additions, at least in the form of hydrides, increase growth; growth increases as the density of <c> component dislocation loops increases, but the relationship is not linear; growth out to high fluence is very closely a constant volume process; at high fluence, growth curves of recrystallized and cold worked Zircaloy-2 or Zircaloy-4 intersect. Slides from the oral presentation include:

- Objective:
  - IIG of Zr-alloys is affected by a complex interplay of:
    - Composition (addition of Fe, Nb, Sn, and hydrogen);
    - Fabrication (cold work, texture);
    - Irradiation conditions (T_{irr}, fluence)
    - Impurities (e.g., S, O)
- Approach:
  - Irradiation of several alloy variants in BOR-60 MTR
    - T_{irr} : 320 ± 10°C (applicable to PWRs and BWRs)
    - Maximum fluence (~ 1.7) x 10^{26} m^{-2} (E > 1 MeV) ➔ 37 dpa
    - 57 dpa for certain pre-irradiated specimens

Figure 5-1: Stress-free Irridation Induced Growth (IIG) [Yagnik et al]

- **Confirmed: Adding Nb to Zr lowers grow**
- **Zr with just Sn has the highest growth of all RXA or SRA or cold-worked materials in program**
- **In most cases, accelerated growth occurs above about**
  7-10 X10^{21} n/cm^2 (E>1Mev, PWR/BWR), or ~ 11-17 dpa
- **Fe and H hydrides have strong influence on growth**

Figure 5-2: Important results – reasons "Why?" being determined [Yagnik et al]

Alloy (Axx)	Growth, %	comment
Zr1Sn.1Fe	2.6	
Zircaloy -4	1.74	Large grain, C, S?
Zircaloy-2	1.34	70% cw
Zircaloy-2	1.23	
Zircaloy-4	1.09	
Zr1Nb.1Fe	0.5	
Zr1Nb1Sn.1Fe	0.4	

Figure 5-3: Ranking of Growth of programs materials at ~ 2X10^{22} n/cm^2 E>1MeV (BWR/PWR equivalent grain size 6-8 microns, RXA (Fe near 1000 ppm)) [Yagnik et al]

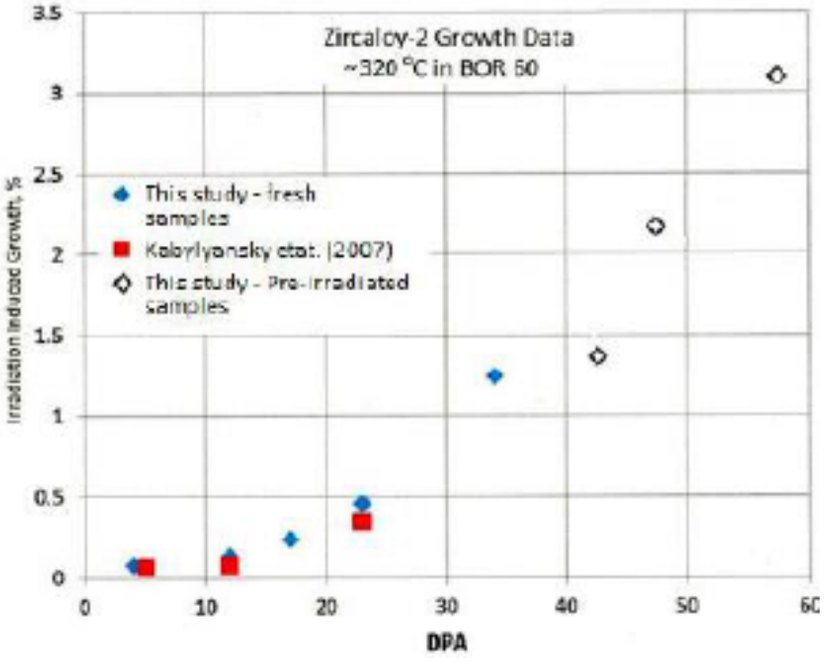

Figure 5-4: Kobylyansky Data Extendened: Ref Zr-2 growth data found to be consistent [Yagnik et al]

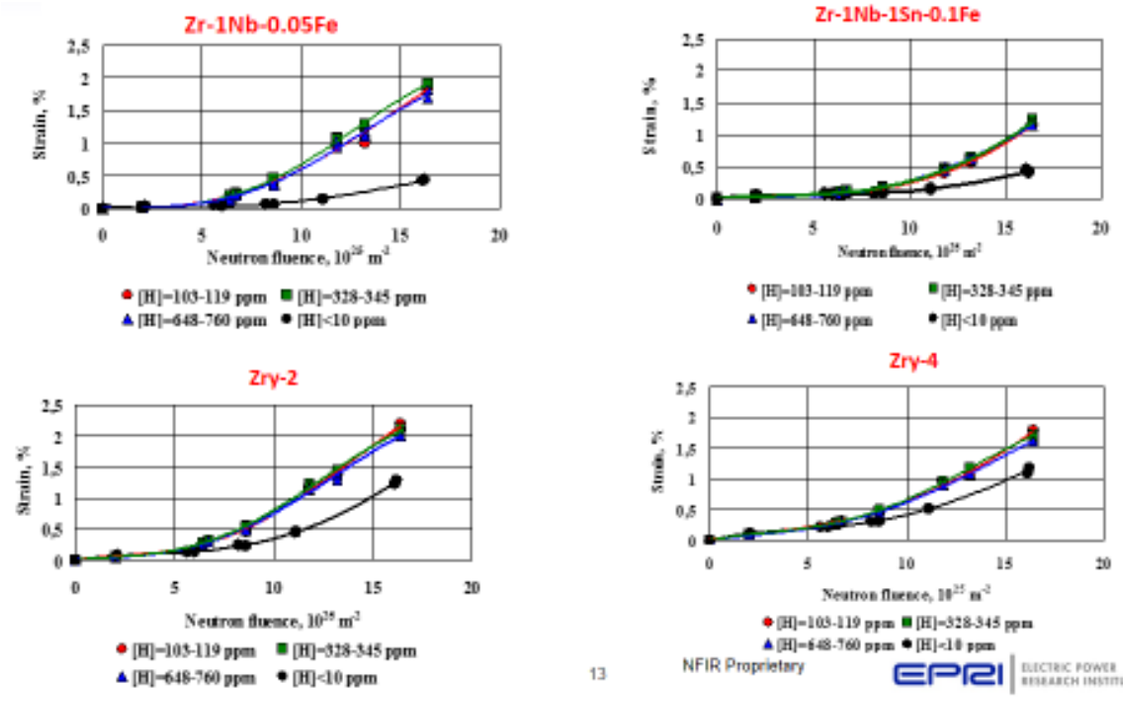

Figure 5-5: Irridation-induced growth strain of pre-hydrided samples vs neutron fluence [Yagnik et al]

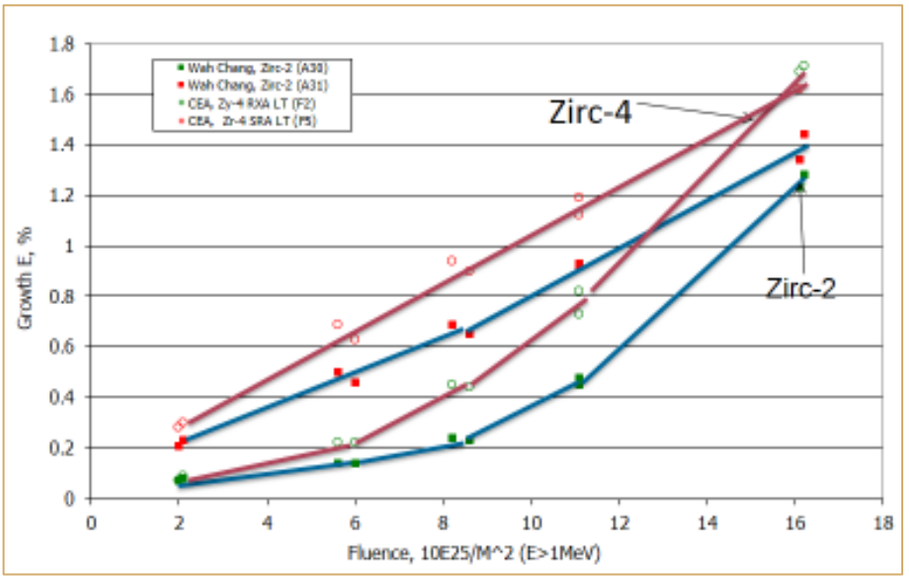

Figure 5-6: RXA and SRA specimen growth converges at high BOR 60 fluence [Yagnik et al]

6 Corrosion and Hydriding (F. Garzarolli)

6.1 Recent publications on mechanistic studies

6.1.1 Oxidation mechanism out reactor

Uniform corrosion of Zr alloys in water and steam proceeds by a cyclic mode, exhibiting in most cases a cyclic rate transitions after certain time-, respectively, oxide thickness-intervals, ~2 µm. There is still no generally accepted root cause model for the cyclic corrosion rate transition. Microstructural examinations of the oxide layer are consequently being motivated and sponsored by different collaboration programs as the Westinghouse led MUZIC-2 research program.

Oxygen ingress during corrosion results in a complex microstructure at the metal/oxide (M/O)-interface:

- *an oxygen diffusion zone in the underlying metal,*
- *a zone with an O content above the O-solubility of the metal.*
- *one of the lower stoichiometry oxide phases (e.g. ZrO) at the M/O interface,*
- *potentially? an amorphous ZrO_2 interlayer at the M/O interface,*
- *fine equiaxed ZrO_2 grains at the M/O interface usually tetragonal but in some cases also monoclinic (in samples with nodular oxide),*
- *columnar grains in the barrier layer, with a more or less developed texture, oriented in the growth direction with a length and diameter depending on the corrosion rate,*
- *a zone with equiaxed grains at the portion in the oxide corresponding to the transition from low to very high rate corrosion rate*
- *an outer porous part of the oxide layer and an inner dense part (barrier layer) governing the corrosion rate via the barrier layer thickness*

[Hu et al 2015] reported on a study of oxide phases in the oxide layer, especially at the M/O interface, of Zr0.9Nb0.08Fe corroded in 360°C water for 360 days, with very modern technics. Figure 6-1 (a) shows a bright field (BF) image of the TEM sample. Below the Pt layer, which is used to protect the sample during milling, a ZrO_2 layer of thickness 2.8 µm exist. The oxide layer consists of equiaxed grains on the outer surface and columnar grains towards the metal/oxide interface. Some lateral cracks are visible throughout the oxide, the largest near the metal/oxide interface. The dark-field image of the same area in Figure 6-1(b) shows metallic second phase particles (SPPs) embedded in the oxide with voids above them. Below the M/O interface, large Zr metal grains are visible in both images, with embedded metallic SPPs. These SPPs are β-Nb and $Zr(NbFe)_2$ particles. A similar general microstructure has been seen in oxidized Zr alloys in many previous examinations.

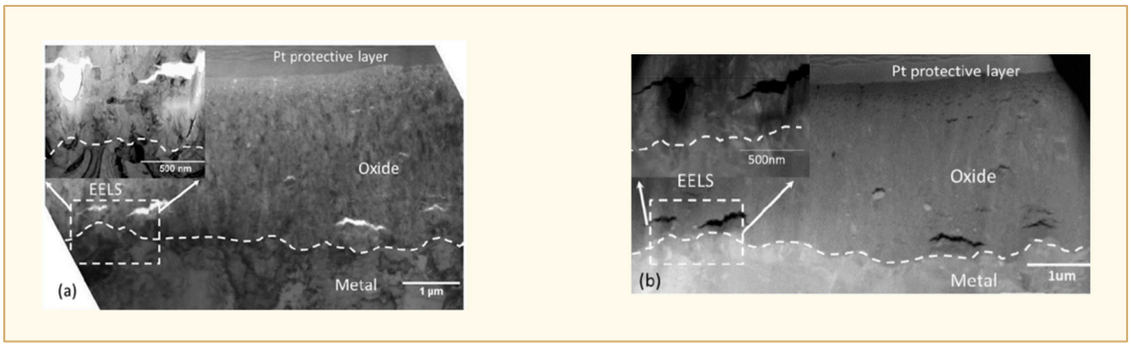

a) Bright field image b) Dark field image

Figure 6-1: TEM image of the oxide film formed on Zr0.9Nb0.01Sn0.08Fe in 360°C water for 360 days [Hu et al 2015]

Close to the metal/oxide interface just between the two cracks the TEM bright field image in Figure 6-2(a) a strongly diffracting suboxide grain was seen, which is highlighted by dotted lines. The diffraction pattern indicates that the suboxide grain is hexagonal ZrO.

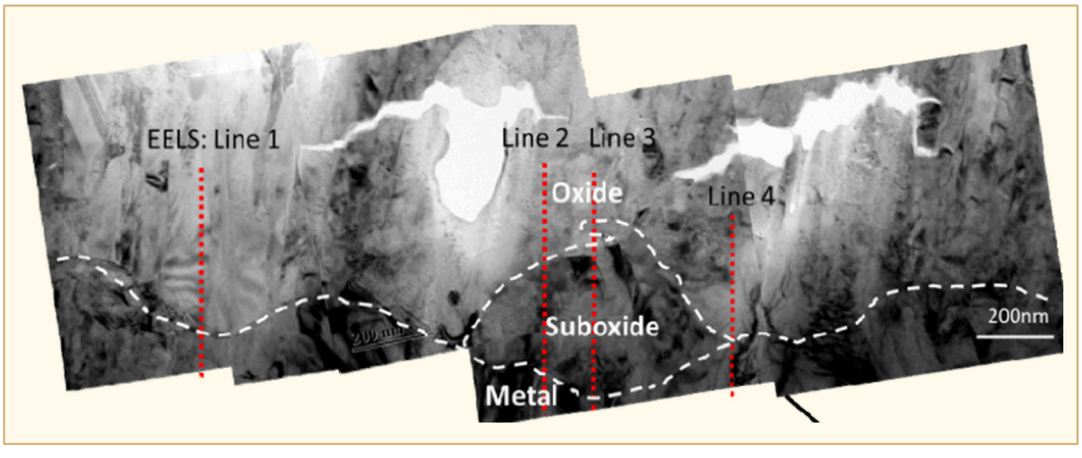

Figure 6-2: High magnification TEM bright field image of the area near the meta/oxide interface. The suboxide grain is highlighted using dotted lines [Hu et al 2015].

The phase map from the transmission Electron Backscatter Diffraction (t-EBSD) analysis, shown in Figure 6-3 highlights the typical oxide microstructure, with small equiaxed grains at the outer surface and large, elongated monoclinic grains towards the interface, oriented parallel with the oxide growth. At the interface, blocky grains are clearly visible, indexed as hexagonal ZrO phase.

Comparing these observations with data from other Zr alloys, it appears that this sample (Zr0.9Nb0.08Fe) has a thicker suboxide layer than faster corroding alloys such as ZIRLO.

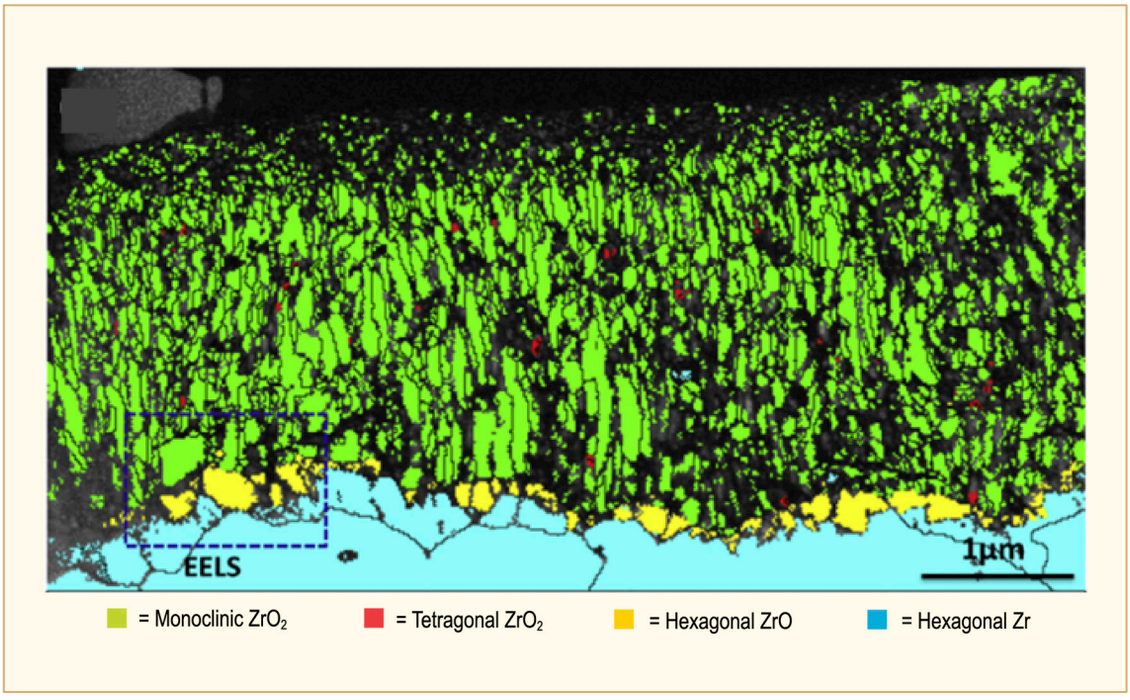

Figure 6-3: Phase map from t-EBSD analysis of the TEM sample (grain boundaries >10° are highlighted [Hu et al 2015].

The structure at the M/O-interface has been studied previously by [Motta et al. 2005, Yilmazbayhan-2006, Dong et al. 2013, and de Gabory et al. 2015]. They examined Zircaloy-4, ZIRLO, Zr2.5Nb and Zr0.4Fe0.2Cr via TEM, by EELS and via APT tomography. Three different phases are seen at the metal side of the O/M-interface during the pretransition period:

1. a small intermediate suboxide layer identified as a cubic ZrO phase (containing 45-50% O),
2. an oxygen-saturated layer ($Zr(O)_{sat}$ layer), containing up to 35% O) with blocky grains found at some places along the interface, with diffraction patterns indexed as Zr_3O [de Gabory et al. 2015] or as Ω-Zr [Bossis et al. 2000],
3. and a region in which the oxygen content is in solid solution and slowly decreases into the metal (less than 30 at. % O).

The width of these interfacial regions depends on the alloy and the stage of corrosion (Figure 6-4). It decreases markedly at transition, likely because the high corrosion rates at transition do not allow them enough time to form. Within the blocky 'suboxide' grains at the O/M interface sometimes fine tetragonal ZrO_2 grains were found.

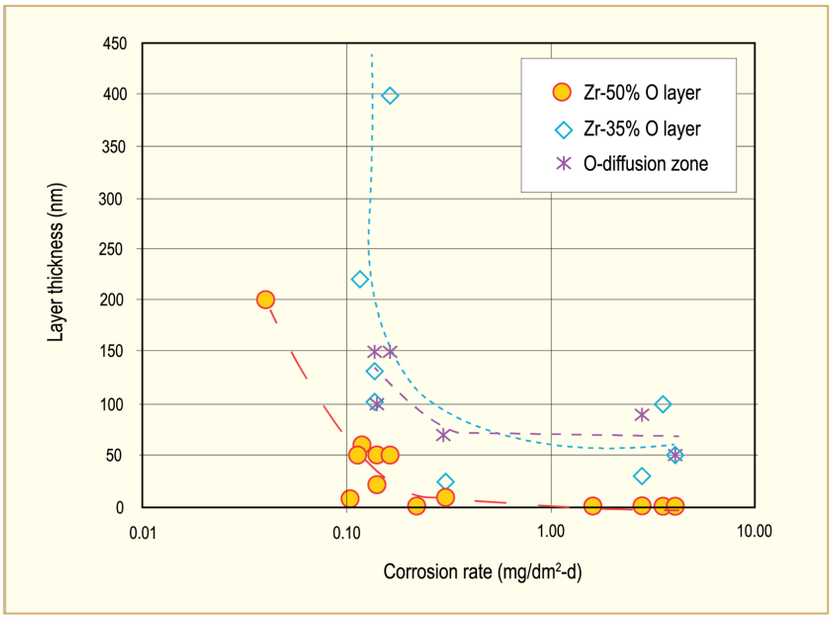

Figure 6-4: Thickness of ZrO-, Suboxide-, and Diffusion-zones after corrosion of different Zr alloys in 360°C for different exposure times (before and after transition). Data from [Dong et al. 2013, de Gabry et al. 2015 and Preuss et al. 2011]

[de Gabory et al. 2015] illustrated the evolution of the oxygen-containing phases at the M/O interface for Zircaloy-4 and ZILO oxidized in 360°C water (Figure 6-5). According to his examinations pre-transition the sub-oxides are generally of variable thicknesses (0-80 nm) and do not form continuous layers. The $Zr(O)_{sat}$ layer is generally thicker (150–200 nm wide). After transition, the ZrO layer has largely disappeared. Small ZrO fingers were occasionally observed. Whether fingers exist or not is believed to be related to the rate of advance of the oxide front.

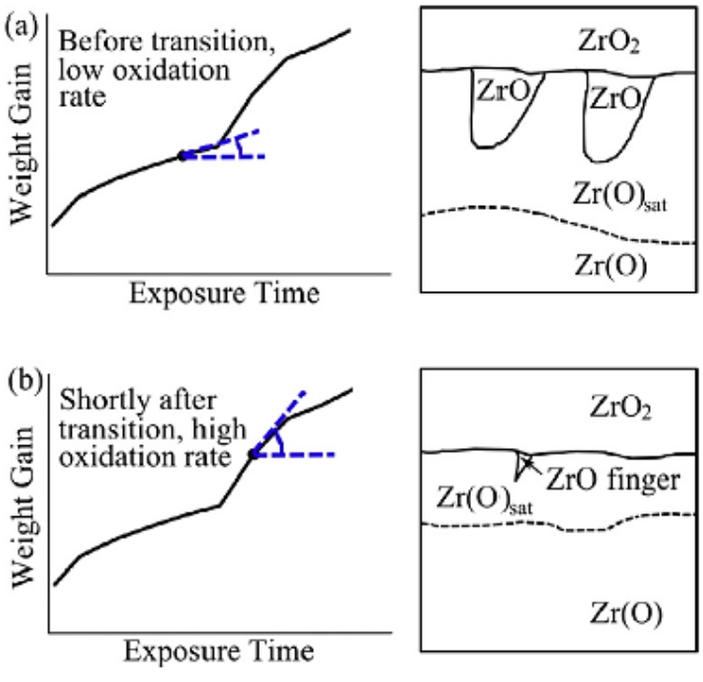

Figure 6-5: Schematic illustration of oxygen containing phases present at M/O interface in (a) pre-transitioned and (b) post-transitioned samples [de Gabory et al. 2015].

The conclusions related to the Zr-oxide layer structure formed close to the M/O-interface in case of the uniform and nodular corrosion vary somewhat. According to [de Gabory et al. 2015] small tetragonal oxide grains nucleate at the beginning of the Zr-oxide formation at the M/O-interface because of the stabilization of the tetragonal phase by the small grain size (possibly aided by high stress and oxide sub-stoichiometry) relative to monoclinic afforded Some of these small grains are properly oriented for growth (they have their $(110)_t$ or $(110)_t$ planes parallel to the O/M-interface.) As these grains grow, they become columnar and when they pass the critical diameter of ~30 nm they transform to monoclinic oxide, maintaining the same orientation during further growth. The monoclinic columnar grains, properly oriented with $(200)_m$ near the oxide-growth direction, grow into the metal. The nodular oxide layer, formed at 500-520°C/105-125 bar, has been observed to contain equiaxed grains, globular pores, and large horizontal cavities and has a very loose structure [Garzarolli et al. 1991]*It is well known that the corrosion is significantly increased once a massive hydride rim forms on the surface of a Zr alloy cladding.* [Jublot et al. 2016] reported on studies of pre-transition oxide layers (~1.2 µm) formed on Zircaloy-4 coupons and Zircaloy-4 coupons with a 8 µm thick massive hydride ($ZrH_{1.66}$) layer in 360°C water. The diameter of the columnar grains was observed to be significantly smaller on ZrO_2/Hydride than on ZrO_2/Zry-4 samples. *It is well known that oxygen diffuse in Zr-oxide layers preferentially through grain boundaries.* They concluded that the higher corrosion in case of massive hydride rims is at least to some extent due to the finer lateral grain diameter. Certainly it has to be remembered that a significant corrosion increase in case of samples with a massive hydride rim usually occurs especially after the corrosion rate transition e.g. [Garzarolli et al. 2001]

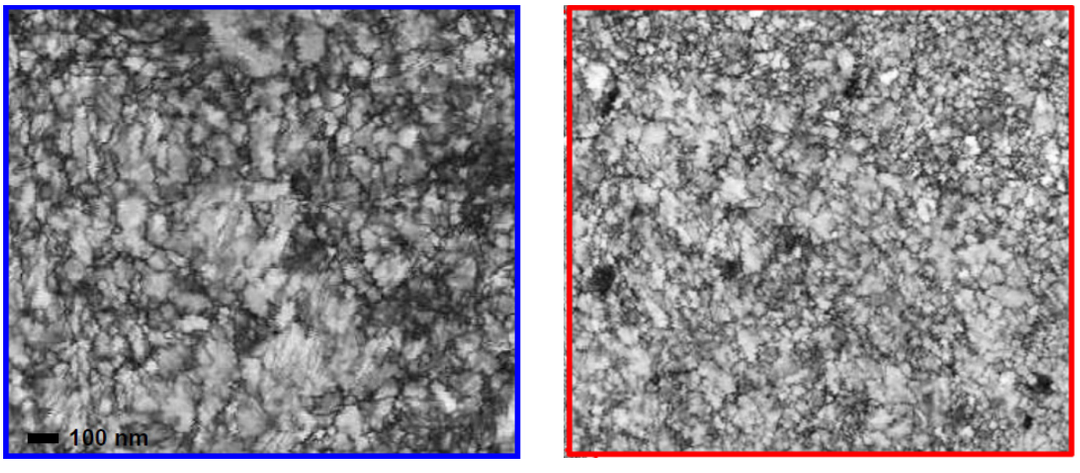

a) ZrO_2/Zry-4 sample b) ZrO_2/Hydride sample

Figure 6-6: Diameter of the columnar grains observed on ZrO_2/Hydride than on ZrO_2/Zry-4 samples [Jublot et al. 2016]

6.1.2 Oxidation mechanism in reactor

The state of knowledge on the mechanism of irradiation induced changes of Zr alloy corrosion is very small. In the last year results from several now ongoing studies was reported.

In PWR after some time Zircaloy-4 exhibits a rate transition with an irradiation induced increase of the corrosion rate. Proposed reasons include:

(a) irradiation induced microstructural changes in the metal, e.g. amorphization and dissolution of second phase precipitate Laves phases,

(b) degradation of the oxide barrier layer e.g. through degraded nucleation and growth of zirconia crystallites as affected by Fe-enhanced diffusion,

(c) changes in the conductivity of zirconia by gamma radiation, resulting in the ejection of electrons to the conduction band and some enhanced electronic conduction, called radiation-induced conductivity (RIC),

7 Primary failure and secondary degradation – open literature data (P. Rudling)

The open literature data are provided in the following sections.

7.1 Introduction

7.1.1 Primary failures

During reactor operation, the FR may fail due to a primary cause such as fretting, PCI manufacturing defects, corrosion, etc. (Table 7-1).

Table 7-1: Primary failure causes for LWR fuel during normal operation and Anticipated Operational Occurrences (AOO).

Primary failure cause	Short description
Excessive corrosion	An accelerated corrosion process results in cladding perforation. This corrosion acceleration can be generated by e.g., CRUD deposition (CILC)[a], Enhanced Spacer Shadow Corrosion, (ESSC)[b], (in BWRs), dry-out due to excessive FR bowing.
Localised hydriding	Fuel may fail in hydrided regions fractured under tensile loading that arose with accumulation of exposure during the course of normal operation (BWRs)[c]. Li seems to be involved in the failure mechanism (It is not clear from where the Li originated since Li does not normally occur in BWR coolants). More work is needed to understand the mechanism that led to the localised hydriding.
Manufacturing defects	Non-through-wall cracks in the fuel cladding developed during the cladding manufacturing process. Defects in bottom and/or top end plug welds. Primary hydriding due to moisture in fuel pellets and or contamination of clad inner surface by moister or organics. Too large a gap between the FR and the spacer grid supports (poor spacer grid manufacturing process) leading to excessive vibrations in PWR fuel causing fretting failures. Chipped pellets may result in PCI failures both in liner and non-liner fuel.
PCI	PCI – an iodine assisted SCC phenomenon that may result in fuel failures during rapid power increases in a FR. There are three components that must occur simultaneously to induce PCI and they are: 1) tensile stresses—induced by the power ramp, 2) access to freshly released iodine-occurs during the power ramp, provided that the fuel pellet temperature becomes large enough and 3) a sensitised material—Zircaloy is normally sensitive enough for iodine stress-corrosion cracking even in an unirradiated state.
Cladding collapse	This failure mechanism occurred due to pellet densification. This failure mode has today been eliminated by fuel design changes and improved manufacturing control.
Fretting	This failure mode has occurred due to: Debris fretting in BWR and PWR. Grid-rod fretting – Excessive vibrations in the PWR FR causing fuel failures. This situation may occur for example due to different pressure drops in adjacent FAs causing cross-flow. Baffle jetting failures in PWRs – Related to unexpectedly high coolant cross-flows close to baffle joints.

[a] CILC – an accelerated form of corrosion that has historically resulted in a large number of failures in BWRs. Three parameters are involved in this corrosion phenomenon, namely: 1) Large Cu coolant concentrations as a result of e.g., aluminium brass condenser tubes, 2) Low initial fuel rod surface heat flux – occurs in Gd rods and 3) Fuel cladding that shows large initial corrosion rates- occurs in cladding with low resistance towards nodular corrosion.

[b] This corrosion phenomenon resulted in a few failed rods. The mechanism is not clear but seems to be related to galvanic corrosion. This corrosion type may occur on the fuel cladding in contact or adjacent to a dissimilar material such as Inconel. Thus, this accelerated type of corrosion occurred on the fuel cladding material at spacer locations (the spacer springs in alloy BWR fuel vendors fuel are made of Inconel). Water chemistry seems also to play a role if the fuel cladding material microstructure is such that the corrosion performance is poor. Specifically coolant chemistry with low Fe/(Ni±Zn) ratio seems to be aggressive (provided that the cladding material shows poor corrosion performance. A fuel cladding material with good corrosion resistance does not result in ESSC, even in aggressive water chemistry.

[c] Sixty-three GE13B 9×9 fuel assemblies in Browns Ferry, Unit 2 (BF2) during Cycle 12 failed. Seven rods were examined in hot cell to determine the primary failures cause.

ANT International, 2014

Table 7-2 and Table 7-3 provide key data for some of the most recent fuel-failure cases.

Table 7-2: Summary of previous PWR/PHWR failure key events, see previous ZIRAT/IZNA-reports for details. New results added to the table from the ZIRAT18/IZNA13 AR [Rudling et al, 2013] is in red text.

Nuclear unit	Type of primary failure	Comment
TMI-1, Cy 10, 1995	Nine high peaking FRs, Zry-4 Cladding, failed after 122 days of operation. CRUD/corrosion related failures.	All failed and degraded pins reportedly had Distinctive CRUD Pattern (DCP)[21]. High peaking factors, thermal-hydraulic conditions. Calculations indicated that no boiling should have occurred on the pins with DCP, although the pins with DCP were calculated to have a slightly higher temperature. Water chemistry (low pH at BOC, pH < 6.9, max LiOH 2.2 ppm). Some, AOA effect was found reaching a maximum in the middle of cycle 10. The source of the CRUD could not be determined. The CRUD sampling showed that the nickel-to iron ratio was in the range 1.25 to 16.7, which was reportedly somewhat lower than in previous investigations.
Seabrook, Cy 5, 1997	Five one-cycle ZIRLO rods failed. CRUD/corrosion related failures.	Longer cycle in transition to 24-month cycle. Possibly CRUD-induced overheating resulting in substantial nucleate boiling.
EdF data reported in 2009 [Thibault et al, 2009]	The main failure causes in the EdF plants are: GTRF wear, Clad manufacturing defects and, Excessive fuel assembly bowing (resulting in assemblies grids hanging-up during loading and unloading and IRI)	A significant number of fuel failures were related to the M5 fuel cladding in 1300 MWe and 1450 MWe units. The M5 FR failures were due to fabrication defects either related to the end plug girth or fill hole weld or defects in the fuel clad itself at grid levels (related to the pulling of the rods into the assembly structure). To resolve these manufacturing issues, AREVA has modified the welding techniques as well as the rod pulling procedure. It was observed that there were no GTRF failures in 2008 (in previous years there have always been some GTRF failures). The reasons for the great improvement is thought to be due to that both AREVA and Westinghouse have introduction reinforced FAs design (AFA3GLr – AREVA and RFA2- Westinghouse). Since the introduction of the AREVA AFA3G design in 1999, a decrease of the average core bow in EdF NPPs has been observed, especially on the 900 MW units, but not as fast as expected. The maximum values of bowing remain relatively high on the 1300 MW units, typically between 15 and 19 mm for a “S shape” bow. The Westinghouse RFA fuel design behaves in the same way with similar bowing range while HTP assembly deformations are twice less. Incomplete Rod Insertions (IRIs) due to bowing have been significantly reduced since the AFA3G FA’s design has been loaded in EdF NPPs and despite the increasing of the average discharge burnup of the FAs. In 2008, no anomaly of RCCA drop time was observed in EdF NPPs during the BOC tests. Concerning the EOC tests, no anomaly was observed in the 12 feet units whereas four RCCAs dropped without recoil in the 14 feet units. Three of them was AFA3G FAs (two “2nd cycle” FAs and one “4th cycle” FA) and one was the older design (AFA2G). The number of FAs damaged during handling operations has decreased in 2008 but remains significant. The damages concern only AFA 2G or 3G design and mainly the 14 feet units. It occurs during the unloading operations. The damages generally occur during a “three-sided box” extraction and result from grids’ hanging due to bowing and to a reduced gap between FAs following unexpected grid growth due to re-crystallized Zircaloy-4.

[21] This acronym implies that the fuel inspection revealed CRUD deposits on the fuel rod and that the deposits were uneven in the rod circumference.

Table 7-2: Summary of previous PWR/PHWR failure key events, see previous ZIRAT/IZNA-reports for details. New results added to the table from the ZIRAT18/IZNA13 AR [Rudling et al, 2013] is in red text. (cont'd)

Nuclear unit	Type of primary failure	Comment
Kakrapara Atomic Power Station (KAPS) unit#2, India	Manufacturing defect	A PHWR fuel rod with an incomplete fusion end plug weld. The fuel rod operated at very low power for the first 18 months as the fuel bundle was in a peripheral location of the core during that period. For the next 5 months, the fuel pin operated at a linear power rating of 410 W/cm when the fuel bundle was shifted to a high flux location in the core. In total the rod operated in failed condition for a period of 710 days and accumulated a burnup of 4400 MWd/tU. See ZIRAT18/IZNA13 AR for more details.
Korean PWR plant, identification not known	2 debris-induced fuel failures	PWR debris-induced fuel failures on a thrice-burned fuel rod, not showing any degradation and a first-burned fuel rod, which degraded. See ZIRAT18/IZNA13 AR for more details.
		ANT International, 2012

Table 7-3: Summary of previous BWR failure key events, see previous ZIRAT/IZNA-reports for details. New results added to the table from the ZIRAT18/IZNA13 AR [Rudling et al, 2013] report is in red text.

Nuclear unit	Type of primary failure	Comment
KKL	1997, 1998	Excessive Shadow Corrosion on LK II Zry-2 Cladding under the Inconel x-750 grid springs. The oxide thickness was locally above 500 µm. The most notable cladding corrosion attacks were found on fuel that had experienced a fourth, fifth, or sixth operational cycle. Zn-injection. Low level of Fe in coolant.
River Bend	Cy 8, 1999	At least 12 GE First cycle FRs were failed. Heavy CRUD – The failures appeared in bundles with a significant iron CRUD deposition. The heavy deposits almost filled the gaps between the FRs. Some 700 pounds (320 kg) iron was estimated to have been input to the River Bend-1 RPV during cycle 8 (1998-1999). CRUD deposit thickness in the range 37–55 mils (940 – 1400 µm) was reported. Analysis of the CRUD showed that the major phases were hematite and spinel, reportedly magnetite or zinc ferrite. Significant amounts of copper, up to 15% were found in some cases. No NMCA. Zn-injection.
Vermont Yankee, 2001-2002	5 FRs failed due to CRUD corrosion.	A total of 5 failed GE rods in 4 bundles were removed from the core at Vermont Yankee in a mid-cycle outage in May 2002, along with 40 other bundles deemed most at risk of failure due to being similar to the leakers in terms of duty, exposure, and tubing material.
Browns Ferry 2, Cy 12, 2001-2003	63 FAs failed due to localised massive hydriding	Affected fuel was GE13B claddings that failed in their second cycle with burnups of 29-30 MWd/kgU. Bundles that failed tended to be leading for the reload batch, indicating some impact of duty on tendency for failures. HWC started in BOC Cy 11 and NMCA at EOC 11 was implemented (3/01), Depleted Zinc Oxide (DZO) started in 1997 at 3 to 5 ppb. Maximum oxide thickness both in lower and upper part of the failed rods. Maximum CRUD deposition towards the bottom of the rods. BF2 changed out their condenser tubes to Ti-tubes 8-10 years ago. Cladding material - Corrosion behaviour was sensitive to alloying content, primarily iron and tin; - Multiple ingots were affected; - Ingots supplied by two different vendors were affected. An update of the root cause examinations of the sixty-three failed GE13B 9X9 fuel assemblies in Browns Ferry, Unit 2 (BF2) during Cycle 12 was presented. Seven rods were examined in hot cell to determine the primary failures cause. The authors, [Lutz et al, 2012] and [Lutz et al, 2013] suggest that the BF2 Reload 10 fuel failed by hydrided regions fractured under tensile loading that arose with accumulation of exposure during the course of normal operation. The results also suggest that Li contributed to the failures at least by aggravating the late stage corrosion of the BF2 Reload 10 rods, regardless of any role it may have had in initiating the corrosion. See ZIRAT18/IZNA13 AR for more details.

Table 7-3: Summary of previous BWR failure key events, see previous ZIRAT/IZNA-reports for details. New results added to the table from the ZIRAT18/IZNA13 AR [Rudling et al, 2013] report is in red text. (cont'd)

Nuclear unit	Type of primary failure	Comment
Browns Ferry 3, Cy 11, 2002-2004	3 FAs failed due to localised massive hydriding	DZO started in 1995 at 3 to 5 ppb, NMCA at EOC 9 was implemented and HWC started in BOC Cy 10, DZO went to 5 to 10 ppb after the HWC was started. Affected fuel was GE13B claddings that failed in their third cycle with burnups of 43-47 MWd/kgU. Rod oxide thickness peaked at lower and upper part of the rods but maximum oxide thickness was found in upper part of the failed rods.
River Bend, Cy 11, 2003	7 rods failed due to CRUD related corrosion.	Water chemistry apparently within specification. Cy 11 – No NMCA but HWC and Zn-injection, also high Cu coolant content was observed. First cycle fuel with burnup ranging from 14.6-19.0 MWd/kgU. Siemens ATRIUM-10 (LTP). All failed rods were on periphery in FA on bladed surfaces (high power positions). Failures and peak oxide thicknesses in span 2 (of peripheral rods) where max. CRUD deposition was noted.
Hatch 1, Cy 21, 2003	PCI related failures in five (5) liner (barrier) FRs	Five duty related FRs failed at 19 months into a 22 month cycle in one cycle GE14 barrier fuel with an estimated burnup of 26 MWd/kgU.
Fitzpatrick, 2004	PCI related failures in two (2) non-barrier fuel	Two duty related failures occurred in non-barrier GE12 assemblies late in their second cycle at a burnup of about 45 MWd/kgU.
Kuosheng 2, 2003-2004 (Cycle 16) [Chiu et al, 2009]	PCI related failures in three (3) liner (barrier) FRs suspected to be due to MPS	Duty related failures in two ATRIUM-9B fuel bundles, KAG115 and KBH069 in Cycle 16. The estimated bundle burnup of KAG115 and KBH069 was 28.87 GWd/MTU and 28.64 GWd/MTU respectively. Poolside examinations showed that both bundle had one failed rod at the F2 location. KAG115-F2 failed rod exhibited secondary degradation including a 470 mm axial crack resulting in some fuel washout. The KBH069-F2 failed rod exhibited three defects including a blister, a bulge and, a 5 mm long circumferential crack – fuel washout was noted. A similar fuel failure to those reported above occurred in Cycle 14
Several BWRs	Excessive fuel channel bowing	[Cantonwine et al, 2010] reported on the measured settle times at Monticello and Peach Bottom 3 and compared to the data collected at LaSalle 1. To quantify control rod interference, the amount of interference was calculated in two ways: 1) A Channel Interference Metric (CIM) is defined as the total deflection of both channels toward the blade minus the available gap and 2) the Half-Gap Channel Interference Metric (HGCIM) is defined as the total deflection of an individual channel side minus the available half gap. [Cantonwine et al, 2010] concluded that the new data fits well into the previously developed correlation (reported in ZIRAT14/IZNA9 AR [Adamson et al, 2009b) which showed that an interference (the sum of all 4 blade wings) of <0.5 mm (20 mils) correlated to normal or near normal settling times, 0.5 to 1.0 mm (20 to 40 mils) correlated to slow or no-settle conditions and >1.0 mm would indicate a no-settle condition. The results of half gap interference (the sum of half gap interference of each channel side that faces the blade) showed that >5 mm (200 mil) half gap interference is necessary before a slow or no-settle condition occurs. Cofrentes have experience of >7 mm measured bow in one channel without friction problems in the cell [Sedano & Mata, 2011]. However friction problems can be expected for bows >5 to 6 mm based on the experience in other reactors. If the maximum fuel channel bow exceeds 4 mm there is a risk that the CR does not settle.
		ANT International, 2012

7.1.2 Secondary degradation

A failed LWR FR may degrade either by developing long axial cracks, splits[22], and/or transversal breaks, or may not degrade at all. Degradation of failed fuel may result in fuel washout. This may occur if the rod degrades to such a point that the water gets in contact with the fuel pellets. Steam will

[22] *Axial split* is a term introduced by *GNF* and represents a failed rod that either has an off gas level larger than 5000 µCi/s or a total crack length that is larger than 152 mm (6 inches).

not result in fuel washout while the water phase can. Normally, utilities are much more concerned about fuel washout than high iodine and noble gas release, because it may take up to 10 years to clean PWR and BWR cores of the tramp uranium resulting from the fuel washout. On the other hand, the high iodine and noble gas activities released from the failed rod will be eliminated at the point when the failed rod is extracted from the core. For more details about degradation mechanisms, see [Strasser et al, 2008].

7.2 Results presented in year 2015-2016

In 2010 a total of 41 leaking AREVA fuel rods were discharged from reactors operating in the US region [Mazurkiewicz S. et al., 2016] while in 2015, zero leaking fuel rods were discharged, Figure 7-1.

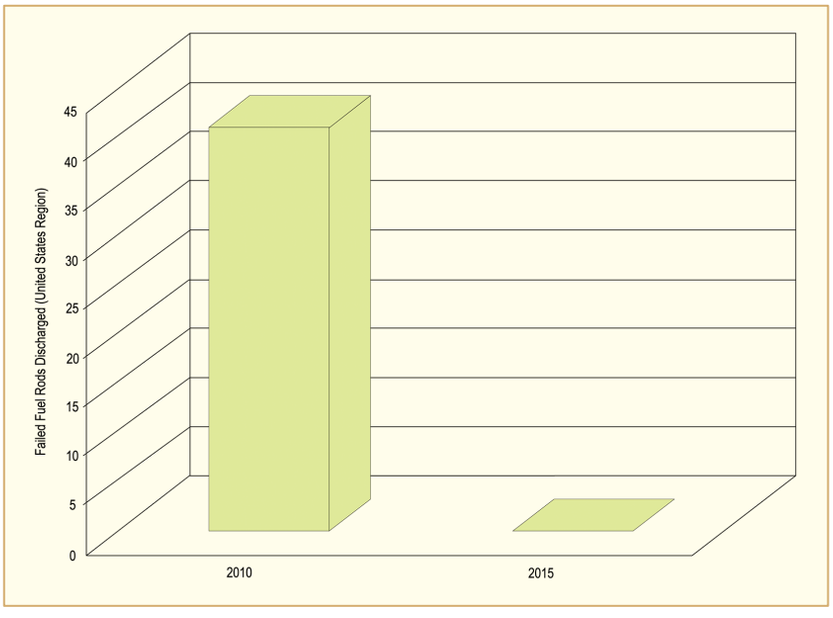

Figure 7-1: Number of AREVA NP Fuel Failures Discharged in US (2010 versus 2015) [Mazurkiewicz S. et al., 2016].

Table 7-4 identifies the mechanisms by which those failed AREVA fuel rods were distributed between BWRs and PWRs.

Table 7-4: Failure Mechanisms (2006 - 2010) [Mazurkiewicz S. et al., 2016]

Rank	BWR (2.6 rods/year)	PWR (26.0 rods/year)
#1	Debris Fretting – 60%	Fretting Wear – 88%
#2	Pellet-Clad Interaction – 40%	Debris Fretting – 5%
#3		Manufacturing –5%
#4		Handling – 2%

Table 7-5 identifies the percent reduction in the top failure mechanisms outlined in Table 2.

8 LOCA, RIA, Seismic event (P. Rudling)

8.1 Introduction

8.1.1 Seismic event

To assure safe operation following a seismic event, additional criteria are defined. Two levels of ground motion excitation, corresponding to two earthquake levels, are defined for safety-related structures, systems, and components in operating nuclear power plants. Compliance with specified criteria assure that plant safely is maintained following each event.

For the first-level earthquake, the Operating Basis Earthquake (OBE), the load factors and acceptable allowable stresses ensure that the stresses in plant structures remain at least 40 percent below the yield stress of the material for the event.

For the second-level earthquake, the Safe Shutdown Earthquake (SSE), whose vibratory motion is usually twice that of the OBE), the associated load factors and allowable stresses ensure that the stresses in the plant structure and assembly remain close to the yield stress of the specific materials; a small excursion in the inelastic range is allowed when the SSE load is combined with accident loads, usually those associated with a LOCA event.

The following criteria relates to a seismic event:

- OBE-Allow continued safe operation of the FA following an OBE event by establishing that the FA components do not violate their dimensional requirements. This is most simply assured by requiring that the stresses in components remain below the yield stress of the unirradiated components.
- SSE-Ensure safe shutdown of the reactor by maintaining the overall structural integrity of the fuel assemblies, control rod insertability and a coolable geometry within the deformation limits consistent with the ECCS and safety analysis. Requirements to assure safe shutdown are:
    - Fuel rod or assembly fragmentation does not occur due to seismic loads.
    - Control rod insertability is maintained by confirming no or small plastic deformation of components.
        - Adequate static and dynamic crush strength of the spacer assembly (PWR/VVER) and fuel channel (BWR), including requirements for Condition III and IV accidents must be ensured. The grid should maintain the fuel rods in a coolable configuration. The seismic criteria are particularly critical since the PWR/VVER spacers and BWR fuel channels absorb the lateral seismic shocks. This means that the hydrogen content in the Zr alloy spacer (PWR/VVER) and fuel channel (BWR) should be limited.
    - Confirmation that the FA (top and bottom nozzles) maintains engagement with the reactor internals.

To ensure that the criteria above are met, fuel vendors limit the maximum allowable amount of hydrogen in grids (for PWRs/VVERs) and fuel channels (for BWRs) to limit the hydrogen embrittlement effect (Figure 8-1). If the hydrogen content becomes too large in these components, the grids or the fuel channel may fracture due to the seismic load making it difficult to insert the control rods and shut down the reactor.

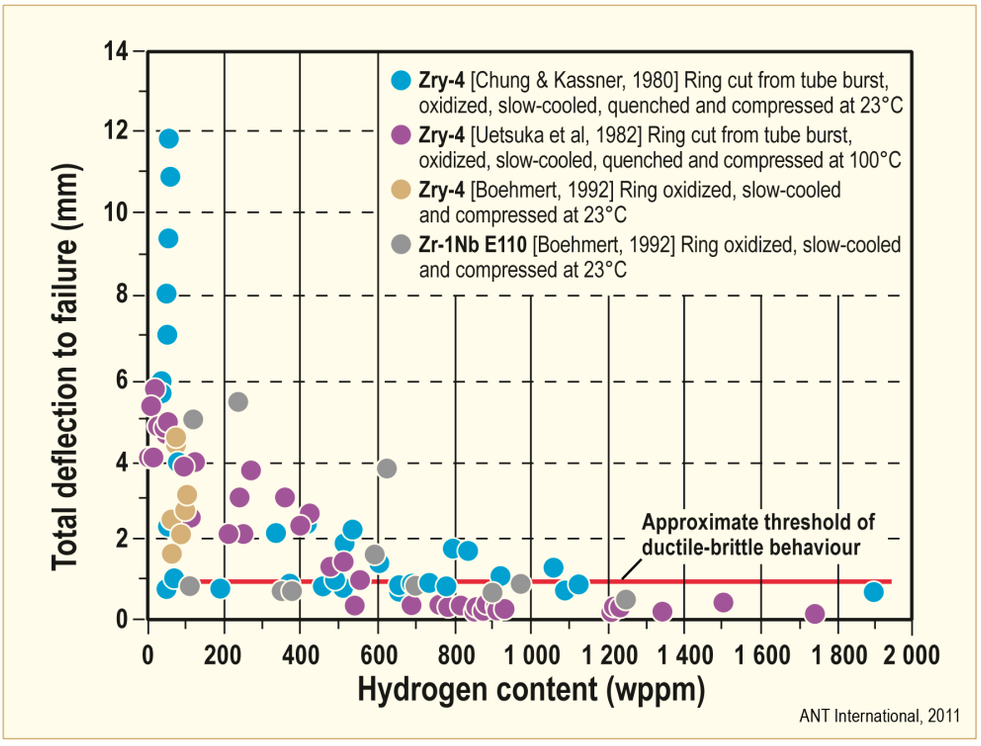

Figure 8-1: Effect of hydrogen on ring compression ductility of unirradiated samples prehydrided before RCT, after [Chung et al, 2001].

Increased burnup may lead to additional HPU through Zr-alloy corrosion of the grids (for PWRs/VVERs) and fuel channels (for BWRs) which may reduce the margins towards satisfactory performance of these components during the seismic event.

8.1.2 Loss of Coolant Accident

The design basis Loss of Coolant Accident (LOCA) is a break in a pipe that provides cooling water to the reactor vessel. Analyses are performed for a variety of break sizes and locations to demonstrate that the ECCS can maintain the fuel in a coolable geometry. The limiting break is typically in one of the cold, main coolant pipes of a PWR or one of the intake pipes to the recirculation pump of a BWR.

The LOCA process starts by the decrease and ultimate loss of coolant flow at the same time that the reactor is depressurized (Figure 8-2). The loss of coolant flow decreases heat removal from the fuel, increasing the fuel temperature and causing a significant temperature rise of the cladding. The decrease in system pressure causes an outward pressure differential and a hoop stress in the cladding wall. The result is the plastic deformation, or *ballooning* of the cladding. Ballooning may also result in *fuel relocation*[23] that may impact the cladding temperature as well as the Equivalent Cladding Reacted (ECR[24]) in the later phase of LOCA.

Ballooning of the fuel rods may result in *blockage* of the coolant sub-channel that in turn may impact the fuel coolability. If large fuel clad burst strains occur at the same axial elevation, *co-planar deformation*, in the FA, the coolability may be significantly degraded. Specifically, the clad azimuthal

[23] Fuel relocation may occur, if during LOCA a section of the fuel rod experiences ballooning, by slumping of fuel fragments from upper location in the ballooned section.

[24] The ECR is defined as the total thickness of cladding that would be converted to stoichiometric ZrO_2 from all the oxygen that are contained in the fuel cladding as ZrO_2, and oxygen in solid solution in the remaining clad metal phase.

temperature gradient will strongly impact the burst strain. The extent of the ballooning is also dependent on:

- Creep strength of the cladding.
- Stress in the cladding and the corresponding strain rate.
- Temperature and the rate of temperature increase.

Depending on the temperature, the cladding ductility and the rod internal pressure, the cladding will either stay intact or may burst which will allow steam to oxidize the fuel clad inner surface. In addition, some of the hydrogen released by the water/zirconium corrosion reaction inside the burst fuel may be picked up by the cladding resulting in very high local hydrogen concentrations (1000-3000 wtppm H). A fuel cladding with such high hydrogen concentrations will be very brittle even though the cladding is not oxidised at all, i.e. ECR is 0. The fuel clad axial temperature distribution will determine the axial elevation of the ballooned and burst fuel rods in the assembly. The axial and azimuthal fuel clad temperature distribution is a result of the heat transfer mechanisms at the surfaces of the cladding.

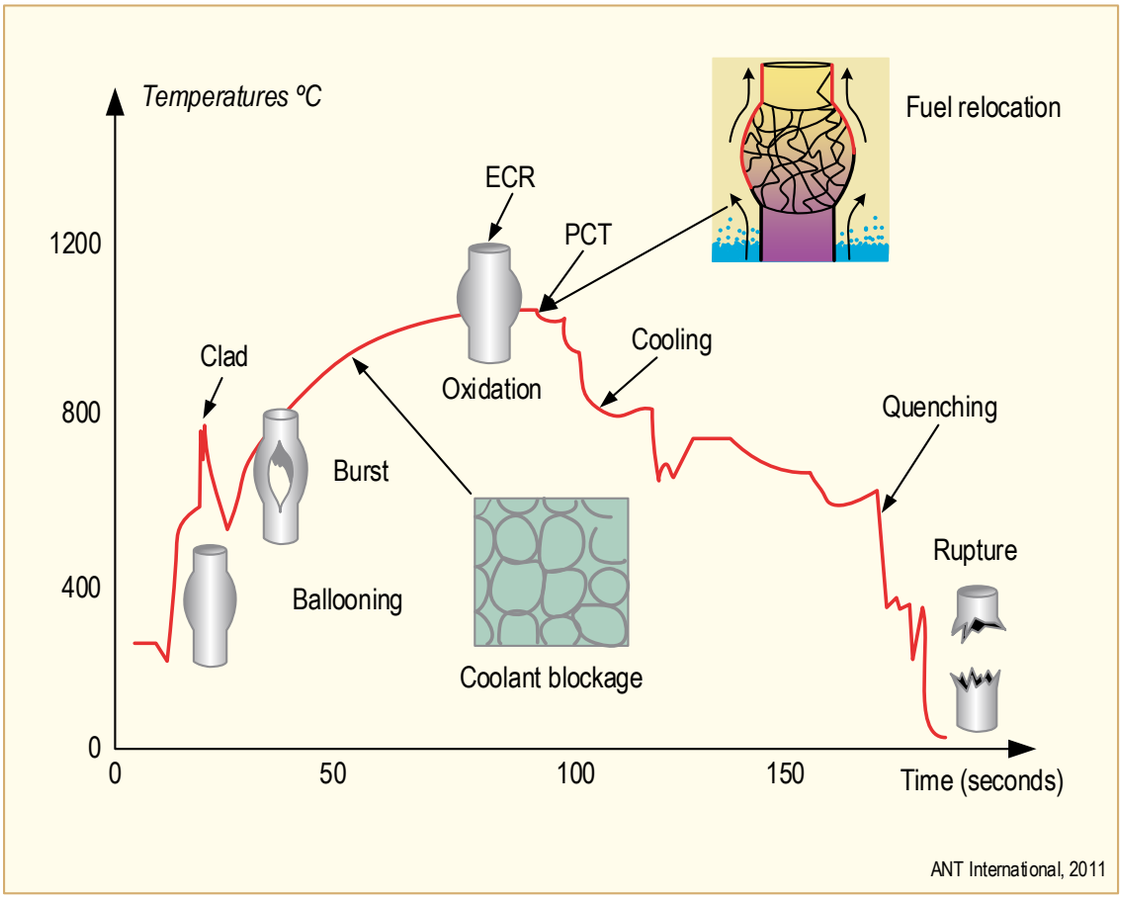

Figure 8-2: Typical LOCA in a PWR.

The increasing temperatures and presence of steam will cause the intact cladding to oxidize on the OD and the burst cladding to oxidize on both the OD and ID (two sided oxidation) until the ECCS is activated and the water quenches the cladding. The oxidation process at the high LOCA temperatures will increase the oxygen and hydrogen content in the cladding, reducing its ductility and resistance to rupture. The process and final structure of the cladding after a LOCA cycle is shown in Figure 8-3.

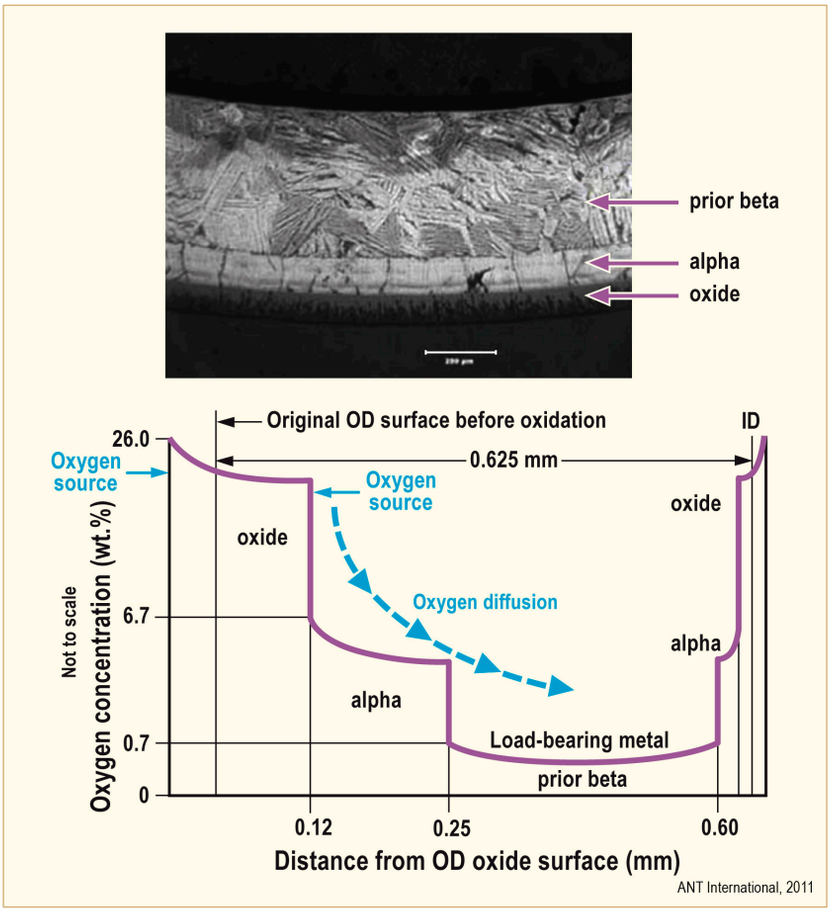

Figure 8-3: Structure of oxidized cladding, after [Meyer, 2013].

- First, the high water and steam temperatures increase their reaction rates with the cladding and increase the conversion of the cladding surface into thicker ZrO_2 films.
- As the LOCA temperature passes the levels where α→β transformations start and finish, the resulting structure consists of:
  - The growing ZrO_2 layer.
  - A brittle zirconium alloy layer with a very high oxygen content which stabilizes the α phase, formed by diffusion of oxygen from the oxide layer.
  - The bulk cladding, which is now in the β-phase, has a high solubility for hydrogen; the hydrogen picked up by the cladding from the water-metal reaction increases the solubility of oxygen in the β layer.
- The ZrO_2 and oxygen stabilized α layers grow with continued diffusion of oxygen and hydrogen from the water reaction. The increasing amount of oxygen convert some of the β-phase to oxygen stabilized α phase with the concurrent shrinkage of the β-phase. The remaining β-phase cladding wall thickness is transformed to α phase, or "prior β-phase", on cooling and is the only structural part of the cladding that can insure its integrity.

During the LOCA oxidation, the first oxide formed is adherent and protective. However, after an extended exposure, *breakaway oxidation* may occur manifested by the change from parabolic to quasi-linear oxidation kinetics and a dramatic increase in HPUF. High temperature oxidation studies have shown that the Zr-Nb materials M5, ZIRLO have similar LOCA oxidation kinetics compared to that of Zry-4, i.e., an intact black oxide layer is preferentially formed which is associated with low HPUF. However, the Russian Zr-Nb alloys E110 and E635 (with similar chemical compositions to

that of M5 and ZIRLO) show a much larger tendency to breakaway oxidation and high hydrogen pickup. It appears that the reason for this difference in behaviour is related to that different source material for E110/E635 (iodide/electrolytic Zr) and M5/ZIRLO (Zr sponge) are used. Also, another reason for the difference in behaviour between these two groups of materials is that the clad outer surface is HF pickled for E110/E635 materials while belt-polishing is used for M5/ZIRLO materials.

The sources and role of hydrogen in the embrittlement of the cladding includes hydrogen from the corrosion reaction during normal operation and hydrogen from the reaction with steam during the LOCA. In addition hydrogen increases the solubility of oxygen and diffusivity of oxygen in the β-phase at high temperatures. Oxygen, in combination with hydrogen, are the two major elements that cause cladding embrittlement by the growth of the α layer and the shrinkage of the structural, prior β layer.

Integrity of the cladding is based partly on the properties of the former β zone, since the ZrO_2 and oxygen stabilized α zones are too brittle to sustain a load. The embrittlement criteria are based on properties of the prior β layer measured on post-simulated LOCA tests of unirradiated Zircaloy-4, by ring compression tests [Hobson & Rittenhouse, 1972] and related to oxidation, or ECR, calculated by the Baker-Just equation. It should be noted that the oxide thickness of the samples were never actually measured during those tests. The United States Nuclear Regulatory Commission (USNRC) accepts ECR calculations by the Cathcart-Pawel equation or others that may be submitted for approval.

The re-entrance of the coolant via the ECCS will quench and cool the cladding. The cladding may rupture due to thermal stresses, or differential expansion of FA components, in the event the cladding ductility is insufficient to accommodate the strain. The cladding temperature will be reduced at a rapid rate (1-5°C/sec) by re-wetting the cladding surface at the Lidenfrost temperature (about 600-700°C). The process will collapse the vapour film on the cladding OD and cooling will be by nucleate boiling. Thermal shock due to the sudden change in heat transfer conditions can fracture the cladding at this stage of the transient. The ability of the cladding to withstand the thermal stresses will depend on the extent of oxidation that occurred during the heat-up stage of the transient. Since, however, all the hydrogen is likely to be in solution at these temperatures, hydrogen is unlikely to contribute to the embrittlement except to the extent that its presence increased the oxygen solubility and increased oxygen content, in turn, increased the embrittled condition of the cladding.

Upon further cooling, the hydrogen stabilized β-phase will decompose below the α-β transformation temperature and the hydrogen will precipitate in the form of hydrides in the α phase and embrittle and potentially crack the cladding. At temperatures of about 135°C/275°F (saturation temperature after the LOCA event) the forces imposed on the FA by the coolant, by handling, by transport and by hypothetical accidents such as seismic events have the potential of cracking the embrittled cladding. The embrittlement effect of hydrogen (in form of hydrides) on ductility during this phase of the LOCA is much stronger than during the quenching phase. The volume fraction of hydrides precipitated will be a function of the cooling rate.

There are several test methods to evaluate the effects of oxidation and quenching on the integrity of the cladding. Integrated tests, or thermal shock tests appear to approach LOCA conditions most closely. Mechanical tests include *ring compression tests*, three point bend tests and Charpy impact tests. The samples used are usually unirradiated, pre-hydrided and oxidized to represent the pre-quench conditions except in the integral thermal shock test, which includes the ballooning and oxidation cycle.

The *thermal shock tests* consist of isothermal heating of the fuel to the selected oxidation temperature and then quenched with water at a selected rate. The electrically heated cladding, usually filled with alumina pellets, is placed in a tube with inlets, usually at the bottom for steam to oxidize and for water to quench the cladding. The fuel rods may be free to expand axially or be restrained. The integral thermal shock test simulates the entire LOCA.

8.1.2.1 Current US regulations

The current regulations intend that modelling of the hypothetical accident will show that rupture of the cladding during the quenching process can be prevented by the application of the regulatory limits.

9 Accident tolerant fuel (ATF) (Tahir Mahmood)

9.1 Introduction

Prior to the accident at Fukushima, the emphasis of advanced LWR fuel development was on improving nuclear fuel performance in terms of increased burnup for waste minimization, increased power density for power upgrades, and increased fuel reliability. Fukushima highlighted some undesirable performance characteristics of the standard fuel system during severe accidents, including accelerated hydrogen production under certain circumstances. Thus, fuel system behavior under design-basis accident and severe-accident conditions became the primary focus for advanced fuels, along with striving for improved performance under normal operating conditions to ensure that proposed new fuels will be economically viable.

Decades of industry research and operational experience have produced an extensive database supporting the performance of LWR fuel during normal power operations and during postulated accident conditions. The nuclear power industry is focused on continuous improvement and reliable operation and deploys design enhancements to the fuel system as they become available. Typically these are small incremental improvements to the current fuel system design, which has been optimized over decades. Boiling water reactors currently use Zircaloy-2, while pressurized water reactors previously used Zircaloy-4 and have now transitioned to zirconium-niobium (Zr-Nb) cladding (M5™and ZiRLO™), with M5™ and ZiRLO™ demonstrating improved corrosion behavior relative to Zircaloy-4. The nuclear industry has made great strides in understanding the Zircaloy/UO2 fuel system with systematic improvement in performance as measured by failed assemblies. This is evidenced by inspection of the timeline in Figure 9-1, which shows the impressive improvement in performance (reduced failure of assemblies) for both PWR and BWR systems. Figure 9-1 also includes the current modes of pin failure, indicating grid-to-rod fretting as major contributor.

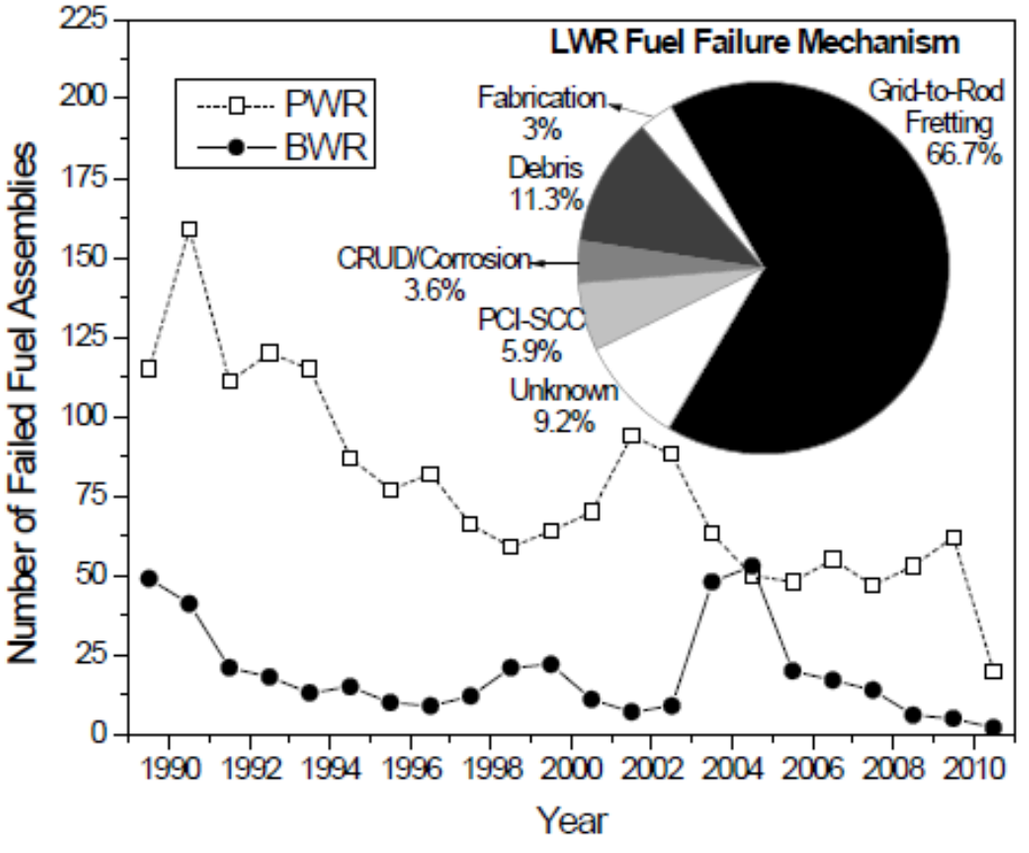

Figure 9-1: Timeline reflecting improved performance in commercial fuel assemblies and breakdown of current pin failure mechanisms in the industry [Bragg-Sitton, 2012].

The development of fuels with enhanced accident tolerance necessarily begins with the definition of down-selection requirements during a concept feasibility assessment. Fuels with enhanced accident tolerance will tolerate the loss of active cooling in the core for a considerably longer period of time and to higher temperatures than the current fuel system while maintaining or improving fuel performance during normal operations. Any new fuel concept proposed for enhanced accident tolerance under rare events must also be compliant with and evaluated against current design, operational, economic, and safety requirements. The complete fuel cycle must be considered, especially for concepts that represent a significant departure from the current technology.

Fuel vendors, nuclear research laboratories, and universities have embarked on an aggressive schedule for the development of enhanced Accident Tolerant Fuel (ATF) systems. The programs are in the early phases of R&D and are currently supporting the investigation of a number of candidate technologies that may improve the fuel system. These ATF systems are being/will be evaluated over all potential "performance regimes" [Bragg-Sitton, 2015]:

- Fabrication/Manufacturability (to include Licensibility)
- Normal operations and anticipated operational occurrences (AOOs)
- Postulated accidents (Design Basis)
- Severe accidents (Beyond Design Basis)
- Used fuel storage / transport / disposition (to include potential for future reprocessing)

In addition to modified/new cladding materials, research is also being done on fuels other than UO_2 as well as new fuel rod designs. This chapter of the annual report provides a brief review of the various ATF systems that are being developed and their current status based on papers published in journals and presentations made at the recent meetings/symposia.

9.2 Overview

Numerous operational and retrofit design changes were instituted in LWRs in the 1980s following the LOCA at Three Mile Island, and these changes have substantially reduced the probability of core degradation during a severe accident. These specific design features and upgrades were primarily associated with maintaining adequate core cooling in the event that the primary cooling system is not functional. The recent station blackout (SBO) accidents at three of the Japanese Fukushima Daiichi reactors following the devastating 2011 earthquake and tsunami have sparked renewed interest in exploring the possibility of further design and fuel system improvements that could improve the safety of LWRs under design-basis (DB) and beyond-design-basis (BDB) accident scenarios.

The accident at Fukushima Daiichi in 2011 illustrated the vulnerability of plants in extended station blackout (SBO) accidents. Explosion of hydrogen gas, primarily from rapid reaction of zirconium-alloy cladding with high temperature, high pressure steam, led to damage of the primary system (Figure 9-2). Melting of the fuel rods accelerated the release and dispersion of fission products outside of the plant boundary.

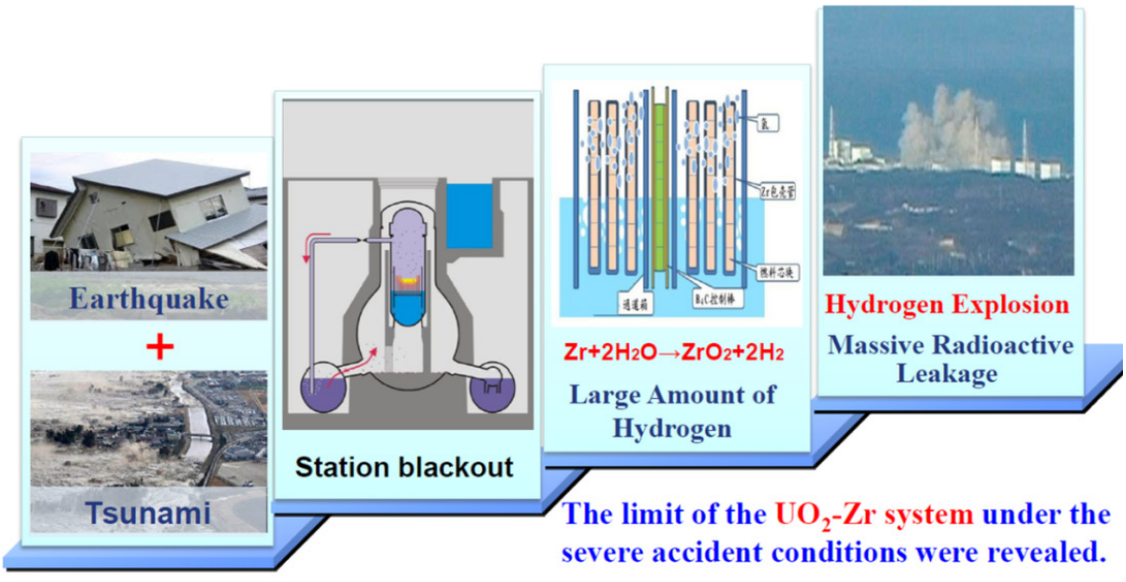

Figure 9-2: Sequence of events at Fukushima Daiichi resulting in hydrogen explosion [Qiu, 2016].

Preliminary evaluations indicate that maintaining availability of passive cooling to remove the decay heat is of utmost importance in preventing rapid fuel rod heat-up in severe accidents. Another defense is to replace the zirconium alloy cladding with an advanced material which can significantly reduce the steam reaction rate and maintain the mechanical integrity of the fuel cladding at high temperatures during a severe accident. An accident tolerant fuel (ATF) cladding can provide additional coping time for plant operators to restore emergency cooling. Fuels with enhanced accident tolerance are, therefore, those that, in comparison with the standard UO2 – Zr system, can tolerate loss of active cooling in the core for a considerably longer time period (depending on the LWR system and accident scenario) while maintaining or improving the fuel performance during normal operations. The key performance features that constitute accident-tolerant behavior are dependent on the specific accident scenario. Figure 9-3 shows the evolution of the fuel rod under a LOCA scenario extending well beyond the design basis limit. The fuel segments in the upper portion of the figure are intended to schematically convey the evolution of the fuel system with increasing burn up (fuel swelling and cracking, fission gas buildup and release, partial oxidation of the clad inner and outer surfaces).

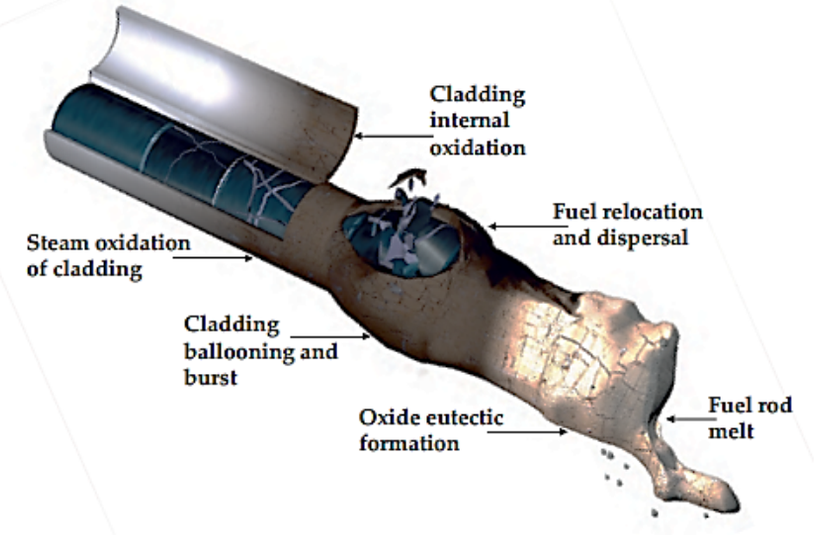

Figure 9-3: Evolution of a fuel rod under LOCA and SBO conditions extending well into the beyond design basis space along with four key performance features of ATF concepts for improved safety margins [Zinkle et al, 2014; Zinkle, 2016].

The major issues that need to be addressed in establishing accident-tolerant fuel attributes are shown in Figure 9-4.

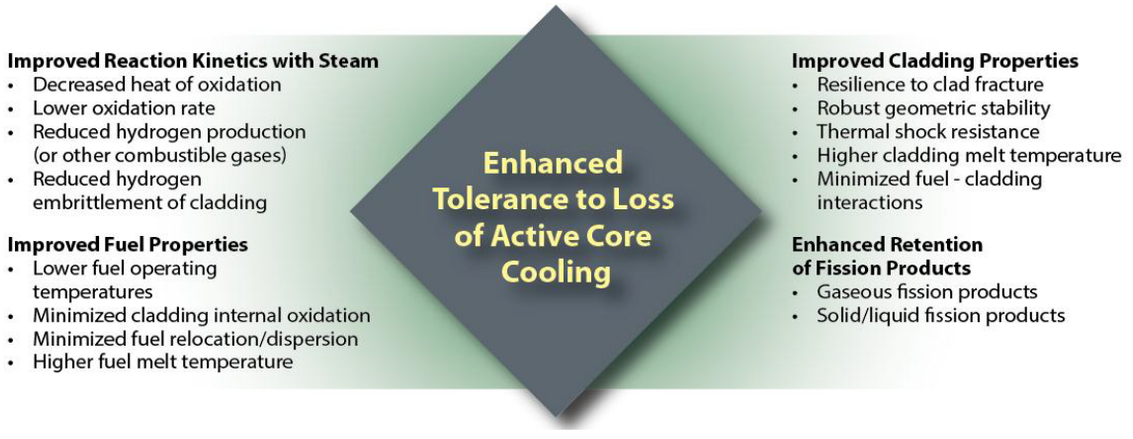

Figure 9-4: Major issues that need to be addressed in establishing accident-tolerant fuel attributes [Bragg-Sitton, 2015].

From review of reports, papers, and presentations, the performance criteria in Table 9-1, Table 9-2 and Table 9-3 were constructed to evaluate potential cladding technologies for further development and testing within the LWR Sustainability (LWRS) Program, [Barrett et al, 2012; ZIRAT20 AR, 2015].

Table 9-1: Identified critical cladding performance parameters which must be met for consideration in further development and testing. See [Barrett et al, 2012] for information about references in the table, after [Barrett et al, 2012; ZIRAT20 AR, 2015].

Critical cladding performance parameters	Zr alloy (standard)	New technology criteria	Comments	Ref#
Maximum operating temp (°C)	650	>650	Temp where structure or oxidation/corrosion becomes limiting	1
Neutron absorption cross section	0.0142 cm^{-1} 0.26 barns	<0.0142 cm^{-1} <0.26 barns	Reduced parasitic absorption	1, 2
U-235 penalty (% increase in U-235 required for equivalent 18 month cycle at constant nominal power)	0	≤0	Equivalent fuel geometry	1
Clad manufacturability (low cost; low complexibilty)	Mfgr 3.05–4.57 ×10^6 m/yr (1); $20-$30 per meter	Mfgr 3.05–4.57 × 10^6 m/yr; (Suggested acceptable increased fabrication costs of up to 50% given power uprates of 10 – 30%) (3)	Must be able to meet current mfg demand – highly complex technologies may be costly and time consuming to manufacture	4
Coolant cladding chemical interaction/degradation	Localized oxidation not to exceed17% of cladding thickness befre oxidation (5)	Not allowed under normal operating conditions of postulated accident conditions		1
Creep (thermal or irradiation)	Creep strain for Zry-4 @ room temp: ~0.66% (7)	≤Zircaloy	Can affect conductivity, fuel clad interactions, and cladding structural integrity	1
Operational lifetime	62 MWd/kg U	>80 MWd/kg U	U-total not U-235. Must be greater than Zr alloy standard	1, 3
Lifecycle net cost of fuel system	8.79 mills/kWeh	<8.79 mills/kWeh	(mill is a unit of measure = 0.001$)	3
High strength/ductility	UTS 437 MPa for Zr4 @ room temp (7)	≥Zr stnd	UTS = Ultimate tensile strength – averaged value between longitudinal and transverse strength	6
Hermeticity			Necessary to contain fission gaes under nominal operating conditions	6
Longer coping times during LOCA	10 hours – dependent on the specific NPP (10 CFR 50.63 & RG 1.155)	>10 hours		8
Hydrogen generation in LOCA (exothermic reaction rate in steam)	Total H production not to exceed 1% of the total amount of H produced if all metal cladding were to react (5)	Minimal H reaction rate		
Power uprates	3411 MWt – typical LWR	10 – 20% increase		3
				ANT International, 2015

Table 9-2: Cladding parameters which are desirable but not mandatory for consideration in further development and testing. See [Barrett et al, 2012] for information about references in the table, after [Barrett et al, 2012; ZIRAT20 AR, 2015].

Desirable cladding performance parameters	Zr alloy (Stnd)	New technology criteria	Comments	Ref#
Melting point (°C)	1843	>2000 desired	Must withstand accident scenarios	1
Density (g/cm^3)	6.56	<6.56	Leads to improved seismic response	1
Heat capacity	0.07 (cal/g/°C) 293 (J/kg/°C)	>0.07 >293	Increases ability of cladding to damp out temperature increases during accidents. Minor effect.	1
Unirradiated thermal conductivity (k) @300°C (W/mK)	17.41	≥17.41		1
Clad swelling	Swelling occurs	≤Zircaloy	At reactor operating fluence and temperature	1
Fission gas release	1 failure/million fuel pins	≤1 failure/million fuel pins	At reactor operating fluence and temperature	4
				ANT International, 2015

Table 9-3: Cladding parameters needed to obtain Nuclear Regulatory Commission (NRC) licensing. See [Barrett et al, 2012] for information about references in the table, after [Barrett et al, 2012; ZIRAT20 AR, 2015].

Licensing criteria	Zr alloy (standard)	New technology criteria	Comments	Ref#
Clad peak temperature limit (°C) (NRC accident limit)	1200	Peak T limit >1200		1
Departure from nucleate boiling issues (PWR)	Not allowed	Not allowed	Increase in power density must be balanced with heat transfer area per volume	1
Storage/transportation/waste disposal			No new waste disposal challenges from activation products	9
Compatible with higher U-235 enrichment	5 wt.% U	>5 wt.% U		9
Withstand longer cycle lengths	18–24 months	≥18 months	Less lost time due to outages	1
Chemical compatibility with LWR components				9
Consistency meet nuclear QA standards				6
Potential for demonstration as a non-fuel component and lead test rod in 5–10 years				4, 8
				ANT International, 2015

The constraints, associated with any commercial nuclear fuel development and deployment, include (Figure 9-5):

- **Backward compatibility** – Proposed fuel concepts should not require modifications to the fabrication plant or host reactor for demonstration irradiation.

- **Operations** – A new fuel system must maintain or extend plant operating cycles, reactor power output, and reactor control. To maintain current operational levels, some proposed fuel system concepts may require higher fuel enrichment.

- **Safety** – The safety and performance of a proposed new fuel system must be at least as good as that of the UO_2–Zr alloy system under normal, operational transient, design-basis accident, and beyond design basis conditions.

- **Fuel cycle**

  - **Front end of the nuclear fuel cycle** – The impact of new fuels and cladding on the front end of the nuclear fuel cycle must be assessed within the framework of current and future regulations and policies.

  - **Back end of the nuclear fuel cycle** – A new fuel system could also have an impact on the back end of the nuclear fuel cycle. The storage (wet and dry) and repository performance of the fuel (assuming a once-through fuel cycle) must not be degraded (including accident conditions such as e.g. cask drop).

- **Economics** – Economics is a key constraint for industry adoption of a new fuel. It is imperative to maintain enhanced performance goals as an economic consideration.

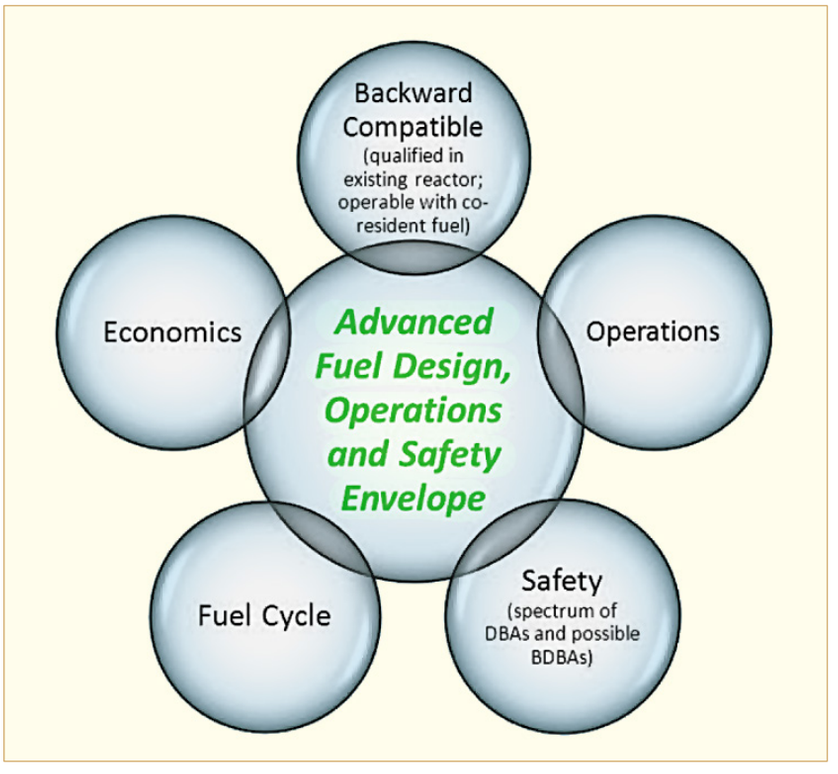

Figure 9-5: Considerations that constrain new fuel designs, [Bragg-Sitton, 2014].

GE-Hitachi (GEH) identified the following safety concerns in an assessment report of advanced material options [GE, 2011] for BWR reactors, but the same requirements can be applied to all current LWR reactors. For Design Basis Accidents (DBA), the primary considerations are related to the cladding as opposed to the fuel form (significant changes in melting temperature notwithstanding):

Design Basis Accidents (DBA)

- **Loss of Coolant Accident (LOCA)** which primarily affects cladding integrity and is influenced by cladding temperature/strength/ductility at temperature, corrosion performance at high temperature, and ability to withstand the thermal loads imposed by Emergency Core Coolant

10 Hydrogen effects during dry storage (C. Patterson and F. Garzarolli, authors; A. Machiels, editor)

10.1 Introduction

The initial assessments in the 1980s and 1990s of the expected performance of commercial spent nuclear fuel (CSNF or simply SNF) during dry storage were based on limiting Zr-alloy cladding degradation by either thermal creep (German approach) or by diffusion-controlled cavity growth (U.S. approach, as documented in the original "Standard Review Plan for Dry Cask Storage Systems," NUREG-1536, Revision 0, issued in 1997). In 1999, the U.S. Nuclear Regulatory Commission (NRC) staff came to the conclusion that "recently developed literature did not support the use of the diffusion-controlled cavity growth model for zirconium-based materials" [ISG-11, Storage of High Burnup Spent Fuel, U.S. NRC Spent Fuel Project Office (1999)], and that NUREG-1536 should be modified to endorse technically defensible methodologies for estimating maximum cladding temperature limits under dry storage conditions.[30] Following issuance of ISG-11, EPRI issued a topical report "Creep as the Limiting Mechanism for Spent Fuel Dry Storage" in 2000 [EPRI, 2000], which also evaluated the potential for cladding degradation by delayed hydride cracking (DHC) and stress corrosion cracking (SCC) in addition to degradation by thermal creep. In July 1992 and November 1993, corresponding to the publication of NRC Interim Staff Guidance 11 (ISG-11), Revs. 2 and 3, respectively, the staff issued, for dry storage applications, a set of generic acceptance criteria applicable to all *commercial* spent fuel burnup levels and cladding materials. However, the staff concluded that, for transportation, reliance on cladding integrity during hypothetical, credible accident conditions of transport required additional information on the impact properties of high burnup cladding material, which could be substantially degraded during dry storage due to phenomena involving hydride re-distribution and re-orientation. Given the impact of hydrogen/hydrides on cladding performance, this section of the Annual Report is intended to focus on the behaviour of hydrogen that can lead to degradation of SNF cladding properties.

10.2 Hydrogen effects

Hydrogen effects pose a concern for the behaviour of Zr alloys not only during in-reactor operations, but also after discharge of the spent fuel assemblies or bundles, particularly during dry storage and transportation. Factors contributing to this concern are:

- Hydrogen has limited solubility in zirconium alloys: Hydrogen in excess of the solubility limit precipitates as hydrides (Figure 10-1) which are brittle, having low critical stress intensity factors of 1 $MPa*m^{0.5}$ to 5 $MPa*m^{0.5}$ between 20°C and 400°C.
- Hydrogen moves under a temperature gradient to colder regions where it can create significant local concentrations.
- Hydrogen moves due to gradients in mean stress, from regions of low to high mean stress[31].
- Hydrogen can cause a growth of initial cracks by re-precipitation of hydrogen at the tip of a notch under tensile stresses (delayed hydride cracking).

[30] In 1994, EPRI published report TR-103949 "Temperature Limit Determination for the Inert Dry Storage of Spent Nuclear Fuel," in which it was concluded that "Cladding creep is the rate-determining degradation and failure mechanism for setting the maximum allowable temperature limit during inerted dry storage of spent fuel."

[31] Mean stress (σ_m) is the average of the three principal stresses in Cartesian coordinates, with tension defined as positive; i.e., the normal convention of mechanics. Hydrostatic stress (σ_H), which commonly appears in the literature of hydrogen and hydriding, is equal to $-\sigma_m$.

- Hydrides can adversely affect the toughness and tensile ductility of Zr-based components at temperatures that vary with concentration and morphology (orientation and effective continuity), but which may be within the temperature range expected for long-term dry storage.

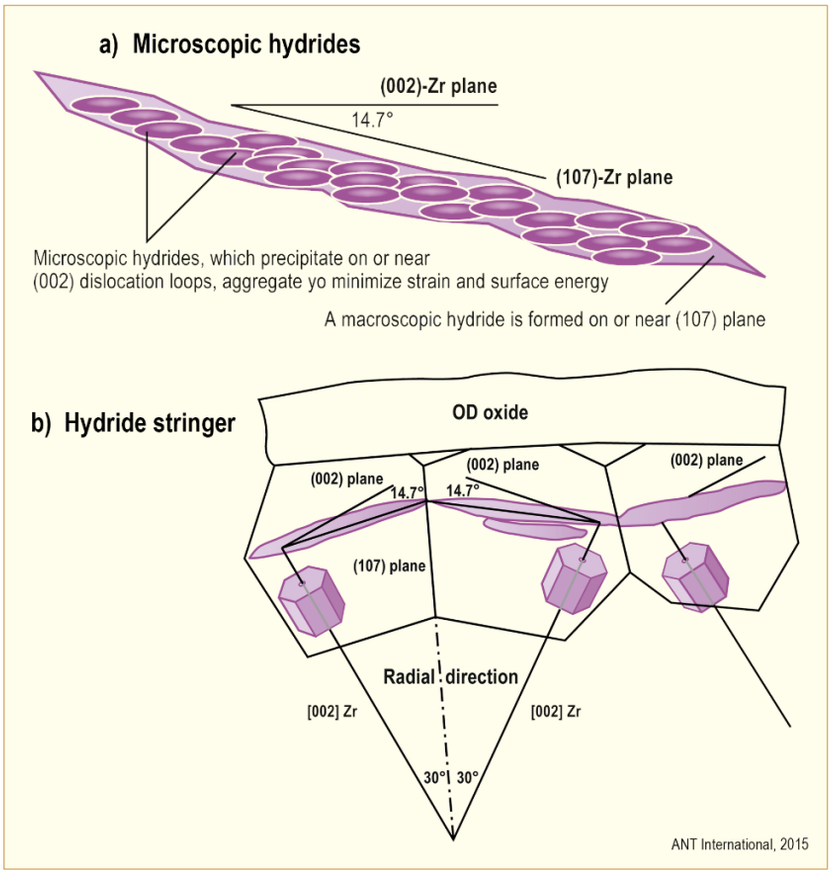

Figure 10-1: Schematic diagrams of a) macroscopic (trans-granular) hydride on the $(10\bar{1}7)$ Zr plane by microscopic hydrides precipitating on the (0001) Zr basal plane and b) hydride stringers consisting of many shorter hydrides closely aligned in a slightly different (zigzag) orientation, after [Chung et al., 2002]

10.3 Hydrogen solubility

The zirconium (Zr) – hydrogen (H) binary equilibrium phase diagram, shown in Figure 10-2, is basic to understanding the relationship between these two elements. For SNF performance, two important aspects are (1) migration and concentration of hydrogen and (2) formation of hydrides. The solubility limit of H in Zr at room temperature is essentially zero (<1 ppm) and increases to only about 60 ppm H to about 200 ppm H at the temperatures of reactor operation and dry storage (300°C to 400°C)[32]. It should be noted that these solubilities refer to the dissolution solvus, TSSD. The dissolution solubility limit represents the concentration of hydrogen, which will be in solution in the spent fuel cladding on heating to the peak temperatures at the beginning of storage. As discussed later in this section, the precipitation solubility limit, TSSP, represents the concentration of hydrogen in solid solution at the lower cladding temperatures that will occur with cooling later in dry storage.

As-fabricated components at room temperature will always contain some hydrides since their initial H concentrations vary in the range of 5 ppm to 10 ppm. At hydrogen levels above the solubility limit, a series of hydrides are formed, which are listed in Table 10-1. The delta and gamma phases are the

[32] The solubilities given here represent the approximate range of dissolution solvus reported in open literature.

most common, most studied, and most discussed in the literature. Recently, during an accurate structural characterization, a new zirconium hydride phase called zeta, ζ, was identified [Zhao et al., 2008]. The ζ phase (Zr_2H) has a trigonal symmetry and is fully coherent with hcp α-Zr. All hydride phases are brittle relative to α-zirconium, having fracture toughness values between 1 MPa√m and 5 MPa√m, as shown in Figure 10-3.

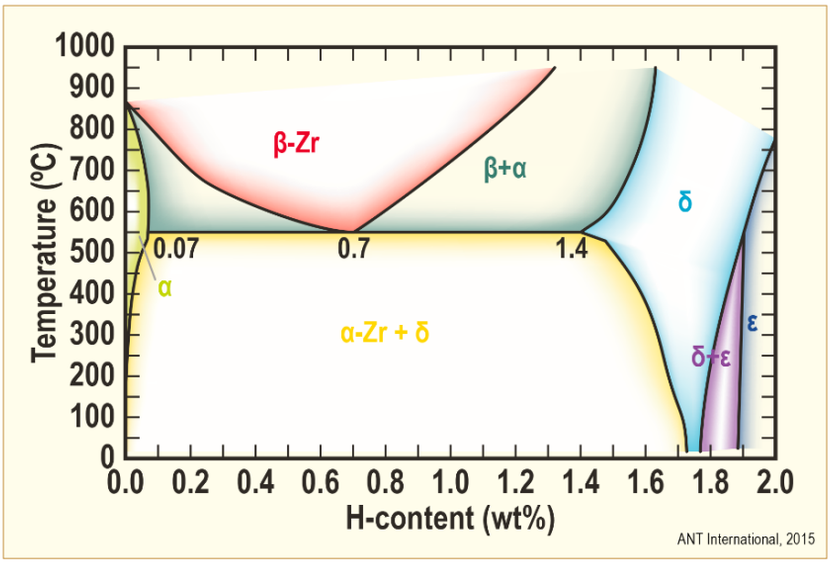

Figure 10-2: Zirconium-hydrogen phase diagram, after [Erickson & Hardie, 1964] and [Kubashewski von Goldbeck, 1972].[33]

Table 10-1: Characteristics of the common zirconium hydrides.

Hydride	Nominal Composition	Composition Range	Crystal Structure	Temperature Range	Volume difference
ε-phase	ZrH_2	1.7-2	fc tetragonal	High & low Ts, but only at very high [H]	
δ-phase	$ZrH_{1.6}$	1.4-1.7	fc cubic	<550°C	ΔV/Vo=16%
γ-phase	$ZrH_{1.1}$	1.1-1.4	bc tetragonal	<180°C	ΔV/Vo=13%
					ANT International, 2014

[33] The body-centered tetragonal "γ-phase", based on the composition ZrH, is not shown in this Zr-H phase diagram. Most workers in the field believe that γ is a metastable phase. However, the case has also been made for a peritectoid transformation:
α-Zr + δ-phase ↔ γ-phase, which can occur at temperatures less than ~250°C.

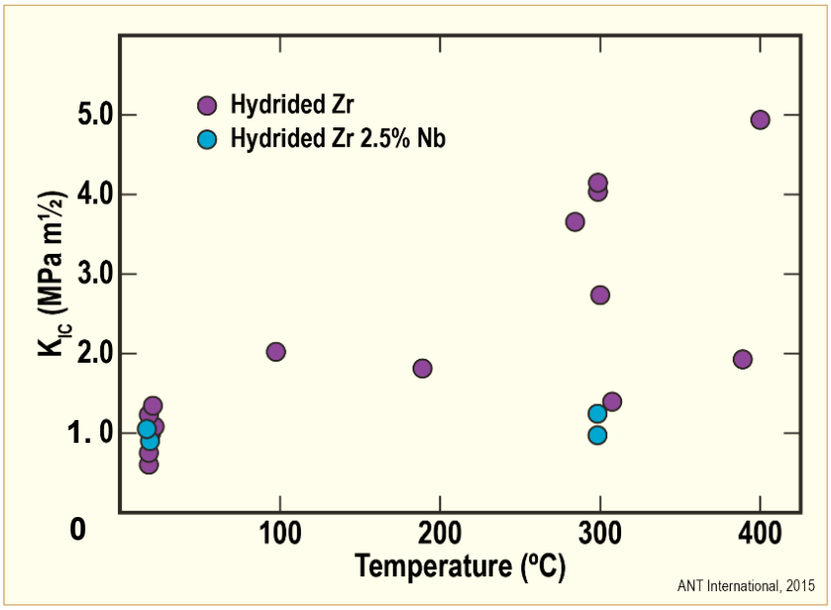

Figure 10-3: Fracture toughness of the δ-phase zirconium-hydride, after [Simpson & Cann, 1979].

In assessments of the behaviour of hydrogen in Zr-alloys, the phase diagram data in Figure 10-2 are more conveniently expressed in the form of solubility diagrams typical of Figure 10-4. Such solubility diagrams contain information from the binary Zr-H phase diagram, but with the temperature and concentration axes interchanged and with principal focus on the lower left corner of Figure 10-2. Hydrogen solubility diagrams typical of Figure 10-4 contain additional information related to the hysteresis observed in measurements of the solubility limits of hydrogen in Zr-alloys. It should be noted that the apparent existence of more than one solubility limit in a binary system conflicts with the basic tenants of thermodynamics. For thermodynamic equilibrium, according to the Phase Rule, composition and temperature cannot be changed independently for two phases to be present in a binary alloy. At a given composition, hydrides should dissolve and precipitate at the same temperature independent of heating or cooling. The presence of two values of the solubility limit indicates that one or both of these values do not represent equilibrium and the hysteresis and values are therefore indicated as “apparent”. In dynamic measurements, values of apparent TSS by heating or cooling are clearly distinguishable and reproducible even if strictly invalid as equilibrium values. They are of practical use for evaluating reactor components and experiments. With this qualification, much of the discussions here will use the presentation type of Figure 10-4 to remain consistent with the literature.

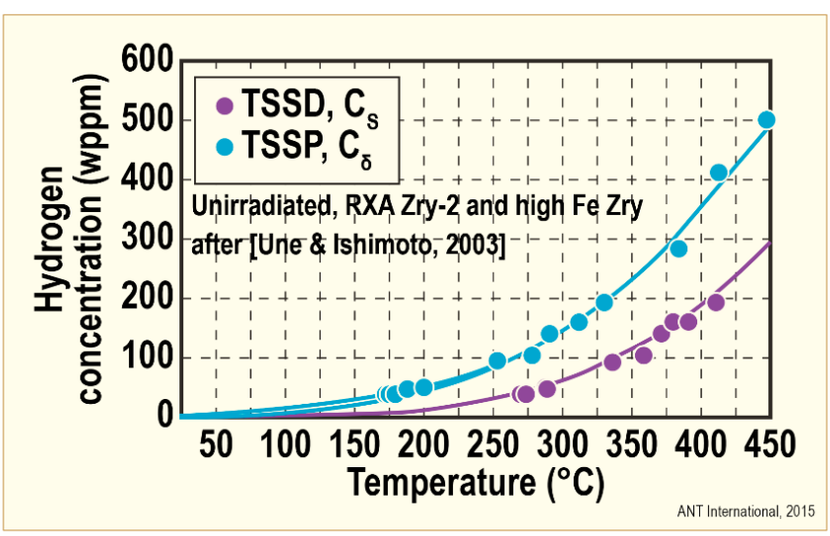

Figure 10-4: Solubility limit of hydrogen in unirradiated Zircaloy on heating (TSSD) and cooling (TSSP); after [Une & Ishimoto, 2003].

As an introduction to the information that follows, the TSSD and TSSP solvi in Figure 10-4 define boundaries between temperature-composition domains in which hydrogen exists in α-phase zirconium as either soluble hydrogen or as both hydrogen and insoluble zirconium hydrides. That is, hydrogen is soluble at temperatures equal to or greater than the TSSD solvus for a given concentration. Alternately, hydrogen is soluble at the concentration given by the TSSP solvus for a given temperature, with any excess existing as hydride phases in the hydrogen-saturated α-Zr matrix (α-Zr(H)).

The behavior of hydrogen in α-Zr(H) with changes in concentration or temperature between the TSSD and TSSP solvi depends, in part, on the absence or presence or hydrides. For the binary hydrogen-zirconium system (all hydrogen in solution), hydrides neither precipitate nor dissolve between TSSP and TSSD. For the system consisting of hydrides in an α-Zr(H) matrix, a third solvus, TSSG, can be constructed between TSSP and TSSD to designate conditions for the growth of existing hydrides. The TSSG in Figure 10-5 was proposed as a hypothetical value based on differences in the volumetric, misfit strain energy needed for the precipitation of a new hydride relative to that needed to grow an existing hydride in an α-Zr(H) matrix, [Une & Ishimoto, 2003]. It is included for reference, but appears to be biased toward the TSSD based on direct measurements that are discussed later in this section. An important aspect of Figure 10-4 and Figure 10-5 is that the diagram separates the concentration of soluble hydrogen (C_H, C_D or C_S), which is diffusible, from the total hydrogen concentration ([H] or C_T). The dependence of TSSP on temperature, especially as temperature decreases, limits the concentration of diffusible hydrogen and reduces hydrogen migration at lower temperatures.

Changes in hydrogen solubility and cladding stress associated with dry storage have the potential for adversely affecting strength, ductility, and, possibly, the integrity of Zr-based components under upset or accident conditions. Information related to these topics is given in the ANT International Dry Storage Handbook (Patterson and Garzarolli), the ANT International topical reports on the effects of hydrides on fuel performance ([Strasser et al., 2008a] and [Strasser et al., 2008b]), the ZIRAT16/IZNA11 Annual Report ([Adamson et al., 2011]) and in other reports such as the assessment of hydride reorientation and damage risk by [Rashid & Machiels, 2007] and the review of the possibility of delayed hydride cracking in SNF by the [IAEA, 2010a] and [EPRI, 2011].

The solubility limit of hydrogen in zirconium alloys increases with temperature as shown in Figure 10-4 and in the alternative representation given in Figure 10-5. As noted above, the terminal solid solubility (TSS) is different when estimated either for dissolution of hydrides on heating (TSSD) or for precipitation on cooling (TSSP). The difference between TSSD and TSSP leads to super saturation of hydrogen during cooling and plays an important role in delayed hydrogen cracking (DHC), which is one of the postulated mechanisms of degradation during dry storage. The solvi also affect hydrogen migration.

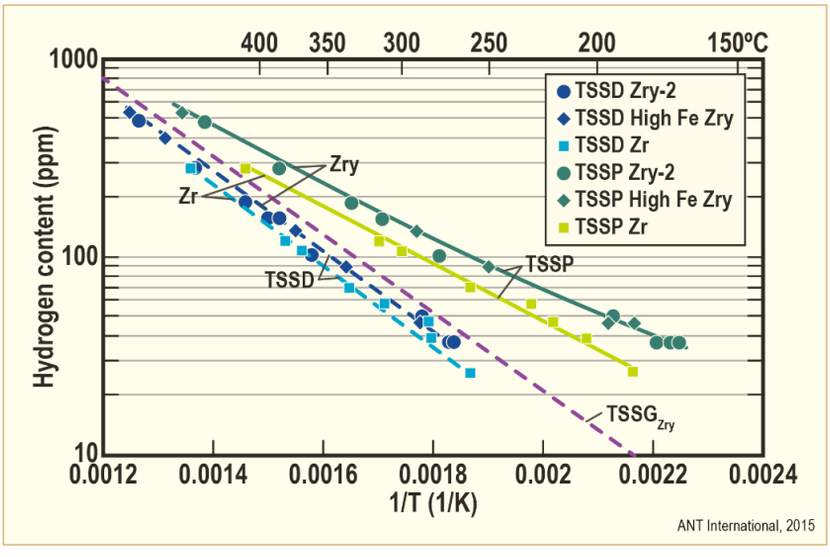

Figure 10-5: Comparison of TSSD and TSSP for unalloyed Zr vs. high Fe Zircaloy 2, after [Une & Ishimoto, 2003].

11 Trends and needs

Improved fuel reliability and operating economics are the driving forces for changing operating conditions, while at the same time maintaining acceptable margins to operating and regulatory safety limits. Table 11-1 gives the trends for Burn Up (BU) achieved compared to regulatory limits in various countries. An approximate ("rule of thumb") conversion of BU to fluence is 50 GWd/MT is equivalent to about 1×10^{22} n/cm^2, E>1 MeV (or about 17 dpa), but this depends on many nuclear parameters such as enrichment, extent of moderation and neutron energy spectrum. In general, PWRs operate to higher discharge BUs compared to BWR because of higher PWR power densities and neutron fluxes, but the differences are decreasing with time. There are some incentives to reach BUs of 60-70 GWd/MT batch average, but the economic values of doing so are decreasing. A majority of US plants and many in Europe have undergone power uprates, from a few percent to up to 20%. This increases the number of Fuel Assemblies (FAs) in a core that operates at high power, thereby decreasing the margin to established limits. In cooperation with utilities, fuel suppliers have operated LTA or LUAs to very high BUs, in some cases approaching 100 GWd/MT peak rod exposures.

Table 11-1: Maximum BUs achieved vs. regulatory limits, (excludes LTAs).

	BU (GWD/MT)				
Country	**Batch**	**Assembly**	**Rod**	**Pellet**	**Regulatory Limit**
USA	57	58	62	73	62.5 peak rod
Belgium		50-55			55 UO_2 assy., 50 MOX assy.
Czech Republic	51	56	61		60 peak rod
Finland	45.6*	48.6	58		57 assy. (for PWR)
France	47	51 UO_2 42 MOX			52 assy.
Germany	58	62	68		65 assy.
Hungary		50	62		
Japan	50	55	62		55 UO_2 assy., 45 MOX assy.
Korean Republic	46				60 rod
Netherlands	52	55	59		60 rod
Russia	60	65			
Spain	50.4	57.4	61.7	69	
Sweden	47	57.2	63.6	65	60 assy., 64 rod
Switzerland	64	68	73		80 pellet
Taiwan					60 rod (P), 54 assy. (B)
UK	44.3	46.5	50		55 pellet
Ukraine		50			
*Current batch design for 50 GWD/MT in BWR					
					ANT International, 2014

As discussed in earlier sections, material properties and microstructure evolve as BU and fluence become higher. Examples include:

In PWRs, Zry-4 no longer meets corrosion and hydriding performance needs; therefore virtually all current PWR cladding now use a zirconium alloy containing Nb.

Although not a new phenomenon, observed Second Phase Particle (SPP) dissolution and re-precipitation phenomena have required a new perspective on alloy development and Hydrogen Pick Up (HPU).

BWR channel bow at high BU has required a new understanding of the relationships between HPU, shadow corrosion and irradiation growth.

A broader listing of issues needing resolution include:

Corrosion related to oxide thickness and H pickup:

- BWRs and PWRs:
  - Effects of solid hydrides on corrosion mechanism.
  - Effect of Nb.
- BWRs:
  - Shadow corrosion mechanisms and its relation to channel bow.
  - Late increased corrosion and HPU of Zry-2 at high Bus – with and without shadow corrosion
  - Kinetics of hydriding in the shadow corrosion-affected channel surfaces
  - Localised hydriding – Browns Ferry – new failure mechanism
  - CRUD-chemistry-corrosion interactions.
  - Effect of water chemistry impurities, as well as specific effects of NMCA, with or without Zn-injection.
- PWRs:
  - Effects of surface contaminations and/or boiling on Zr-Nb alloys.
  - Welding of the new alloys may need improved processes (Zr-Nb alloys).
  - Effect of increased Li together with increased duty (sub-cooled boiling) with and without Zn-injection.
  - Effects of increased hydrogen coolant content (to mitigate Primary Water Stress Corrosion Cracking (PWSCC)).
  - Axial offset anomaly (AOA) mechanisms.
  - Mechanism of improved corrosion due to Nb additions

Mechanical properties related to irradiation and H pickup:

- Decreased ductility and fracture toughness as consequences of the increased HPU and formation of radial hydrides during any situation (e.g., RIA, PCMI, LOCA and post-LOCA events, seismic event, transport container drop-accident conditions).
- Quantification of the effect of irradiation on the apparent solubility of hydrogen, and mechanism by which the phenomenon occurs.
- Details of deformation mechanisms in zirconium alloys, including being able to predict the dislocation channelling system.
- Development of micromechanical models applicable to deformation at appropriate component conditions.
- Mechanism similar to DHC (degradation of failed fuel, outside-in cracking and dry storage).
- Mechanism causing the ductile-brittle transition temperature in zirconium alloys
- Role and kinetics of Fe, Cr, Ni from dissolving SPPs in Zry and Zr-Nb alloys for corrosion, mechanical properties and dimensional stability.

References

Abolhassani S et al., *TEM examinations of metal-oxide interface of Zr based alloys irradiated in Halden reactor*, IFA-638, 18th ASTM Zr conference 2016, Westin Hilton Head, USA

Abolhassani S., Restani R., Rebac T., Groeschel F, Hoffelner W., et al, *TEM Examinations of the Metal-Oxide Interface of Zirconium Based Alloys Irradiated in a Pressurised Water Reactor*, Journal of ASTM International, Vol. 2 (6), Paper JAI12390, 2005.

Abson, D.J., and Jonas, J.J., *Substructure Strengthening in Zirconium and Zirconium-Tin Alloys,* J. Nucl. Mater., 42, pp. 73–85, 1972.

Adamson, R., Cox, B., Davies, J., Garzarolli, F., Rudling, P., Vaidyanathan, S., *Pellet-Cladding Interaction (PCI and PCMI)*, Vol ZIRAT-11 Special Topic Report, Advanced Nuclear Technology International, Skultuna, Sweden, 2006.

Adamson, R., Garzarolli, F., Patterson, C., Rudling, P., Strasser, S., Coleman, C. and Lemaignan, C., *ZIRAT16 Annual Report*, Advanced Nuclear Technology International, Mölnlycke, Sweden, 2011.

Adrian S. Losko, Sven C. Vogel, Mark A.M. Bourke, Stewart L. Voit, Anton S. Tremsin, Kenneth J. McClellan, Andrew T. Nelson, *Neutron characterization of UN/U-Si accident tolerant fuel prior to irradiation*, Top Fuel 2016, Boise, ID, September 11-15, 2016

Amaya M. et al, *Behaviour of High-burnup Advanced LWR Fuels under Accident Conditions*, Top Fuel 2016, Boise, ID, September 11-15, 2016.

Anonymous, Canadian Standards Association, *Technical Requirements for In-service Evaluation of Zirconium Alloy Pressure Tubes in CANDU Reactors,* Update 2, N285.8-10, 2013a.

Anonymous, *Standard Specification for Wrought Zirconium Alloy Seamless Tubes for Nuclear Reactor Fuel Cladding*, ASTM International, B811-07 (Approved 2013b).

Aomi M., Baba T., Miyashita T., Kamimura K., Yasuda T., Shinohara Y., Takeda T.*Evaluation of Hydride Reorientation Behaviour and Mechanical Properties for High-Burnup Fuel-Cladding Tubes in Interim Dry Storage*, Journal of ASTM International, Vol. 5, No. 9, JAI101262, 2008.

Arborelius, J., Backman, K., Hallstadius, L., Limbäck, M., Nilsson, J., Rebensdorff, B., Zhou, G., Kitano, K., Löfström, R., Rönnberg, G., *Advanced Doped UO2 Pellets in LWR Applications*, Water Reactor Fuel Performance Meeting, Kyoto, Japan, Japanese Nuclear Society, 2005.

Armijo, J.S., Coffin, L.E., Rosenbaum, H.S., *Development of Zirconium-Barrier Fuel Cladding*, Zirconium in the Nuclear Industry: Tenth International Symposium,Garde, A.M., Bradley, E.R. (Eds.), Baltimire, Maryland, USA, American Society for Testing and Materials, vol ASTM STP 1245, 1994.

Asher, R., Trowse, F., *The distribution of hydrogen in zirconium alloy fuel cladding: The effects of heat flux*. Journal of Nuclear Materials, 35, pp 115-121, 1970.

Atwood A. R., Mueller A. J., Pan G., and Mitchell D., *Breakaway Oxidation of ZIRLO® and Optimized ZIRLO Cladding per 10CFR50.46c Criteria*, Top Fuel 2016, Boise, ID, September 11-15, 2016

Bacalski C F., Jacobsen G M., and Deck C P., *Characterization of SiC-SiC Accident Tolerant Fuel Cladding after Stress Application*, Top Fuel, Boise, ID, September 2016

Bai G., *Research progress of coating on zirconium alloy for nuclear fuel cladding: A review*, Accident Tolerant Fuel Workshop on System Assessment and Materials, Shenzhen, China, June 2016

Baker Jr L.., Just L.C., *Studies of Metal-water Reactions at High Temperatures III (Experimental and Theoretical Studies of the Zirconium-Water Reaction*, ANL-6548, Argonne National Laboratory, Argonne, Illinois, USA, 1962.

Barberis P., Vauglin C., Fremiot P. and Guerin P., *Thermodynamics of Zr alloys: application to heterogeneous materials*, 17. ASTM International Symposium on Zirconium in the Nuclear Industry, Hyderabad, ASTM STP 1543, Feb. 2015

Bare, W., Torgerson, L., *Dry Cask Storage Characterization Project - Phase l: CASTOR V/21 Cask Opening And Examination*, Idaho National Engineering and Environmental Laboratory, Idaho Falls, Idaho, USA, 2001.

Barrett K., Bragg-Sitton S., Galicki D., Advanced LWR Nuclear Fuel Cladding System Development Trade-off Study, INL/EXT-12-27090, September 2012

Bate, P., *Modelling deformation microstructure with the crystal plasticity finite element method,* Philos. Trans. R. Soc. A Math. Phys. Eng. Sci. 357, pp.1589–1601, doi:10.1098/rsta.1999.0391, 1999.

Beale, J., *Fuel Performance Data*, International Utility Nuclear Fuel Performance Conference, June 22-23, 2016, Charlotte, North Carolina, USA, 2016.

Bell B.C.D., et al., *The influence of alloying elements on the corrosion of Zr alloys*, Corrosion Science 105 (2016) 36–43

Bergmann, U., King, J., *TRITON11™ - Westinghouse 11×11 BWR Fuel Design*, Top Fuel 2016, Boise, Idaho, USA, American Nuclear Society, 2016.

Besch O. A., Yagnik S. Y., Woods K. N., Eucken C. M. and Bradley E. R., *Corrosion behaviour of duplex and reference cladding in NPP Grohnde*, Zirconium in the Nuclear Industry: Eleventh International Symposium, ASTM STP 1295, Bradley E. R. and Sabol G. P., Eds. American Society for Testing and Materials, pp. 805-824, West Conshohocken, 1996.

Besmann, T., McMurray, J., Gaston, B., Simunovic, S., Piro, M., *Modeling Thermochemistry of Fuel and Coupling to Fuel Performance Codes*, Top Fuel 2016, Boise, idaho, USA, American Nuclear Society, 2016.

Billone M, Yan Y., Burtseva T., and Daum R., *Cladding Embrittlement during Postulated Loss-of-Coolant Accidents*, NUREG/CR-6967, ML082130389, July 2008.

Billone M.C, *Assessment of Current Test Methods for Post-LOCA Cladding Behavior, NUREG/CR-7139*, ML12226A182, August, 2012.

Billone M.C., Yan Y., Burtseva T.A., and Meyer R.O., *Cladding Behavior during Postulated Loss-of-Coolant Accidents*", USNRC Report NUREG/CR-7219, ANL-16/09, 2016

Billone, M., Burtseva, T., Einziger, R., *Ductile-to-brittle transition temperature for high-burnup cladding alloys exposed to simulated drying-storage conditions*. Journal of Nuclear Materials, 433, pp 431-448, 2013a.

Billone, M., Burtseva, T., Han, Z., Liu, Y., *Embrittlement and DBTT of High-Burnup PWR Fuel Cladding Alloys*, Argonne National Laboratory, Argonne, Illinois, USA, 2013b.

Bischoff J., Vauglin C., Delafoy C., Barberis P., Perche D., Guerin1d B., Vassault1b J-P , Brachet J-C, Development of Cr-coated Zirconium Alloy Cladding for Enhanced Accident Tolerance, Top Fuel 2016, Boise, ID, September 11-15, 2016

Blake, E.M., *U.S. capacity factors: Keeping the grid stable*: Nuclear News. La Grange, Illinois, USA, American Nuclear Society, vol 58, 2015.

Bossis, P., Lelie`vre, G., Barberis, P., Iltis, X., Lefebvre, F., *Multi-Scale Characterization of the Metal-Oxide Interface of Zirconium Alloys*, ASTM-STP 1354, 2000, Vol. 1354, pp. 918–945.

Boutin S. and Graff S., *A New LOCA Safety Demonstration in France*, Top Fuel 2015.

Brach, E.W., *Cladding Consideration for the Transportation and Storage of Spent Fuel*, USNRC Interim Staff Guidance – 11, Revision 3, Spent Fuel Project Office, 2003.

Brachet, J. C., Saux, M. L., Lezaud-Chaillioux, V., Dumerval, M., Houmaire, Q., Lomello, F., Schuster, F., Monsifrot, E., Bischoff, J., Pouillier, E., Behavior under LOCA conditions of Enhanced Accident Tolerant Chromium Coated Zircaloy-4 Claddings, Top Fuel 2016, Boise, ID, September 11-15, 2016

Bragg-Sitton S. and Carmack W. J., Phased Development of Accident Tolerant Fuel, Top Fuel 2016, Boise, ID, September 11-15, 2016

Bragg-Sitton S., *Advanced LWR Nuclear Fuel Cladding System Development Technical Program Plan.* Light Water Reactor Sustainability Program, U.S. Department of Energy. Idaho Falls, ID : Idaho National Laboratory, External Report. INL/MIS-12-25696, 2012.

Bragg-Sitton S., Carmack W. J., Update on the DOE's ATF development program, Nuclear News, Dec. 2015

Bragg-Sitton S., Development of advanced accident tolerant fuels for commercial LWRs, Nuclear News, March 2014

Bragg-Sitton S., *Overview of the U.S. Department of Energy Program on the Development of Enhanced Accident Tolerant Fuels for LWRs*, 2016 Accident Tolerant Fuel (ATF) workshop on System Assessment and Materials, Shenzhen, June 23–24, 2016

Bragg-Sitton S., Update on Accident Tolerant Fuel and IAEA Technical Meeting on ATF, April 2015

Brandt, R., Neuer, G., *Thermal Conductivity and Thermal Radiation Properties of UO2*, //www.degruyter.com/view/j/jnet.1976.1.issue-1/jnet.1976.1.1.3/jnet.1976.1.1.3.xml.

Brankov, V., Khvostov, G., Mikityuk, K., Pautz, A., Restani, R., Abolhassani, S., *Modeling of Axial Distribution of Released Fission Gas in KKL BWR Fuel Rods during Base Irradiation*, Top Fuel 2015, Zurich, Switzerland, European Nuclear Society, pp 547-557, 2015.

Brankov, V., Khvostov, G., Mikityuk, K., Pautz, A., Restani, R., Abolhassani, S., Ledergerber, G., Wiesenack, W., *Analysis of effects of pellet-cladding bonding on trapping of the released fission gases in high burnup KKL BWR fuels*. Nuclear Engineering and Design, 305, pp 559-568, 2016.

Burton, B., Donaldson, A.T., and Reynolds, G.L., *Interaction of Oxidation and Creep inZircaloy-2*, Zirconium in the Nuclear Industry (Fourth Conference), ASTM STP 681, American Society for Testing and Materials, pp. 561-585, 1979.

Burtseva, T., Yan, Y., Billone, M., *Radial-Hydride-Induced Embrittlement of High-Burnup ZIRLO Cladding Exposed to Simulated Drying Conditions*, Argonne National Laboratory, Argonne, Illinois, USA, 2010.

Campello D., Tardif N. , Baietto M.-C., Coret M., and Desquines J., *Secondary creep behavior of Zr-4 claddings under LOCA Conditions*, Top Fuel 2016, Boise, ID, September 11-15, 2016.

Cann, C.D., and Sexton, E.E., *An Electon Optical Study of Hydride Precipitation and Growth at Crack Tips in Zirconium,* Acta Met., 28, pp.1215-1221, 1980.

Cantonwine P., McCumbee P., Martin K., Ledford K., Lutz D., Fawcett R., Connor M., and DeSilva S., Top Fuel, Boise, ID, September 2016

Cantonwine, P., Lin, Y-P., White, D., and Lutz, D., *The Performance of NSF in BWR operating Conditions,* ASTM Symposium on Zirconium in the Nuclear Industry, Hilton Head, 2016 May.

Cantonwine, P., McCumbee, P., Martin, K., Ledford, K., Lutz, D., Fawcett, R., Connor, M., and DeSilva. S., *GNF Fuel Technology Update,* Top Fuel 2016, Boise, ID, September 11-15, 2016, pp. 409-416.

Cantonwine, P., Schneider, R., Dunavant, R., Ledford, K., Fawcett, R., *GNF Fuel Performance 2015 Update*, TopFuel 2015: Light Water Reactor Fuel Performance Meeting, Zurich, Switzerland, European Nuclear Society, pp 295-304, 2015.

Carpenter, G.J.C., *The Dilatational Misfit of Zirconium Hydrides Precipitated in Zirconium*, J. Nucl. Mater., 48, pp. 264-266, 1973.

Cathcart J.V. et al, *Zirconium Metal-water Oxidation Kinetics IV. Reaction Rate Studies*, U.S. Nuclear Regulatory Commission, ORNL/NUREG-17, Oak Ridge National Laboratory, Tennessee, USA, 1977.

Chambon C., Vaudez S., Heintz J-M., *Study of the U3O8 effect on MOX fuel sintering mechanisms*, Top Fuel 2016, Boise, ID, September 11-15, 2016

Cheng B. et al, Program on Technology Innovation: Coated Molybdenum-Alloy Cladding for Accident-Tolerant Fuel: Progress Report. EPRI, Palo Alto, CA: 2015

Cheng B., Chou P., Topbasi C., Kim Y-J, Armijo S., Do C., Ring P., Fabrication of Rodlets with Coated and Lined Mo-alloy Cladding for Testing and Irradiation, Top Fuel, Boise, ID, September 2016-1.

Cheng B., Kim Y-J, Chou P., "Improving Accident Tolerance of Nuclear Fuel with Coated Mo-alloy Cladding," Nuclear Engineering and Technology, 48 pp. 16-25, 2016-2.

Cheng B., Nuclear sector roadmaps, Nuclear News, Jan. 2014

Chow, C.K., Rosinger, H.E., and Bera, P.C., *Creep behaviour of oxidized Zircaloy-4 fuel sheathing*, Proceedings of the Materials in Nuclear Energy Conference, Huntsville, Canada, September 29-October 2, pp. 112-116, 1982.

Christensen, M., Wolf, W., Freeman, C., Wimmer, E., Adamson, R.B., Hallstadius, L., Cantonwine, P.E., and Mader, E.V., *H in α-Zr and in Zirconium Hydrides: Solubility, Effect on Dimensional Changes and the Role of Defects*, J. Physics: Condensed Matter, 27, 2015.

Chu H., Wu S. and Kuo R., *Hydride Reorientation in Zircaloy-4 Cladding*, Journal of Nuclear Materials, Vol. 373, pp. 319-327, 2008.

Chung H. M., Daum R. S., Hiller J. M., Billone M. C., *Characteristics of Hydride Precipitation and Reorientation in Spent-Fuel Cladding*, ASTM STP 1423, 2002,

Cinbiz, M.N., Motta, A.T., and Koss, D., *Hydride Reorientation in Zircaloy-4 Under Different States of Stress as Studied With In-Situ X-Ray Diffraction,* ASTM Symposium on Zirconium in the Nuclear Industry, Hilton Head, 2016 May.

Colas K, et al., *Microstructure evolution in ion-irradiated oxidized Zircaloy-4 studied with synchrotron radiation micro-diffraction and transmission electron microscopy*, 18th ASTM Zr conference 2016, Westin Hilton Head, USA

Colas K., Motta A., Almer J., Daymond M. and Kerr M., *In-situ study of hydride reorientation kinetics using synchrotron radiation*, 16th ASTM Zr Symposium, Chengdu, China, 2011.

Cole, S., Garner, N., Lippert, H.-J., Graebert, R., Mollard, P., Hahn, G., *Protecting AREVA ATRIUM™ BWR Fuel from Debris Fretting Failure,* Water Reactor Fuel Performance Meeting, Sendai, Japan, Japanese Nuclear Society, p Paper 100164, 2014.

Cole, S., Garner, N., Mazurkiewicz, S., Schoss, V., Mollard, P., *ATRIUM™ 11 Operating Experience*, Top Fuel 2016, Boise, Idaho, USA, American Nuclear Society, 2016.

Cole, S.E., Delafoy, C., Graebert, R.F., Louf, P-H., and Teboul, N., *AREVA Optimized Fuel Rods for LWRs*, TopFuel, Manchester (England), pp. 520-529, 2012

Coleman C. E. and Ambler J. F. R, *Susceptibility of Zirconium Alloys to Delayed Hydride Cracking*, Proc. 3rd Int. Symp. on Zr in the Nuclear Ind., Quebec City, PQ, Aug.10-12, ASTM-STP-633, pp. 589-607, 1976.

Coleman, C., Ambler, J., *Measurement of Effective Solvus Temperature of Hydrogen in Zr--2. 5 Wt.-% Nb Using Acoustic Emission*. Canadian Institute of Mining and Metallurgy, 17, pp 81-84, 1978.

Coleman, C., *Comments regarding ongoing research on hydrogen solubility on heating from TSSD to TSSP*., to Patterson, C., 2015.

Coleman, C.E., Markelov, V., Roth, M., Makarevicius, V., He, Z., Chakravartty, J.K., Alvarez-Holston, A.M., Ali Kanwar Liaqat, Ramanathan, L., and Inozemtsev, V., *Is Spent Nuclear Fuel Immune from Delayed Hydride Cracking during Dry Storage? - An IAEA Coordinated Research Project,* ASTM Symposium on Zirconium in the Nuclear Industry, Hilton Head, 2016 May.

Coleman. C.E., and Hardie, D., *Grain-size Dependence in the Flow and Fracture of alpha Zirconium,* J. Inst. Met., 94, pp. 387–391,1966.

Cordero, Z.C., Knight, B.E., and Schuh, C.A., *Six Decades of the Hall-Petch Effect – a Survey of Grain-Size strengthening Studies on Pure Metals,* Int. Mat. Rev., DOI 10.1080/09506608.2016.1191808, pp.1-18, 2016.

Cox, B., Garzarolli, F., Strasser, A., Rudling, P., *Structural Behavior of Fuel and Fuel Channel Components*, Vol ZIRAT10 Special Topical Report, Advanced Nuclear Technology International, Surahammar, Sweden, 2005.

Crank, J., *The Mathematics of Diffusion*, 2nd ed., Oxford University Press, (1975), 32-47.

Cuet A. et al., *Hydrogen Pickup Mechanism in Zirconium Alloys*, 18th ASTM Zr conference 2016, Westin Hilton Head, USA

Cunningham, M., Simonen, E., Allemann, R., Levy, I., Hazelton, R., Gilbert, E., *Control of Degradation of Spent LWR Fuel During Dry Storage in an Inert Atmosphere* Pacific Northwest Laboratory, Richland, Washington, USA, 1987.

Daum Robert S., Majumdar Saurin, Liu Yung and Billone Michael C., *Mechanical Testing of High-Burnup Zircaloy-4 Fuel Cladding under Conditions Relevant to Drying Operations and Dry-Cask Storage*, Proc. Water Reactor Fuel Performance Meeting, pp. 498-531, Kyoto, Japan, October 2-6, 2005.

Davies, J., Hoshi, E., Zimmerman, D., *Ramp Test Behaviour of High O/U Fuel*. Journal of Nuclear Materials, 270, pp 87-85, 1999.

de Gabory B, Dong Y., and Motta A.T., and Marquis E.A., *EELS and atom probe tomography study of the evolution of the metal/oxide interface during zirconium alloy oxidation*, J. Nucl. mAt. 462, 2015, pp 304-309

Delafoy C. et al., "AREVA Cr2O3-doped fuel: Increase in operational flexibility and licensing margins," in proceedings of the Top Fuel 2015, Reactor Fuel Performance Meeting. Zurich, Switzerland. Sept. 13-17, 2015.

Desquines J. , Drouan D., Guilbert S., Lacote P., *Embrittlement of pre-hydrided Zircaloy-4 by steam oxidation under simulated LOCA transients*, Journal of Nuclear Materials 469, pp. 20-31, 2016

Dixon, W., Massey, F., *Introduction to Statistical Analysis*. New York, New York, USA, McGraw-Hill Book Company, 1969.

Dong Y., Motta A.T., Marquis E.A., *Atom probe tomography study of alloying element distributions in Zr alloys and their oxides*, J. Nucl. Mat. 442, 2013, pp 270-281

Drera S S and Kelly J F, *Accident Tolerant, Non-Oxidizible MOX Fuel Fabrication*, Top Fuel 2016, Boise, ID, September 11-15, 2016

Nomenclature

ADS	Automatic Depressurization System
AE	Acoustic Emission
ANL	Argonne National Laboratory
ANT	Advanced Nuclear Technology
AOA	Axial Offset Anomaly
AOO	Anticipated Operational Occurrences
APT	Atom Probe Tomography
AR	Annual Report
AREVA	French Equipment Manufacturer
ASTM	American Society for Testing and Materials
AT	Axial Tensile
ATEM	Analytical Transmission Electron Microscope
ATP	Atom Probe Tomography
ATR	Advanced Test Reactor
B&W	Babcock & Wilcox
BCC	Body Centered Cubic
BDB	Beyond Design Basis
BE	Back End
BN	Belgo-Nucleare
BNL	Brookhaven National Laboratory
BOL	Beginning of Life
BU	Burn-Up
BWR	Boiling Water Reactor
CANDU	Canadian Deuterium Uranium
CB	Channel Bow
CCT	"C"-shaped ring Compression test
CEA	Commissariat à l'Energie Atomique
CILC	CRUD Induced Localised Corrosion
CIM	Channel Interference Metric
CPR	Critical Power Ratio
CRP	Coordinated Research Project
CRUD	Chalk River Unidentified Deposits
CT	Central Tube
CT	Compact Tension
CVD	Chemical Vapour Deposition
CW	Cold Work
CWSR	Cold Work and Stress Relieved
CZP	Cold Zero Power
DB	Deep Bed
DBA	Design Base Accident
DCF	Dual Cooled Fuel
DCP	Distinctive CRUD Pattern
DFT	Density Functional Theory
DHC	Delayed Hydride Cracking
DNB	Post-Departure from Nucleate Boiling
DNBR	Departure from Nucleate Boiling Ratio
DOE	Department of Energy
DS	Dimensional Stability
DZO	Depleted Zinc Oxide
EB	Electron Beam
EBR	Experimental Breeder Reactor
EBSD	Electron Backscatter Diffraction
ECCS	Emergency Core Cooling System
ECR	Equivalent Cladding Reacted
EDC	Expansion Due to Compression
EdF	Electricité de France
EDS	Energy Dispersive Spectroscopy

EDX	Energy Dispersive X-ray spectroscopy
EELS	Electron Energy Loss Spectroscopy
EFPD	Effective Full Power Days
EOL	End Of Life
EPMA	Electron Probe Micro-Analysis
EPRI	Electric Power Research Institute
ESCP	Extended Storage Collaboration Program
ESSC	Enhanced Spacer Shadow Corrosion
ETR	Engineering Test Reactor
FA	Fuel Assembly
FBR	Fast Breeder Reactor
FC	Fuel Channel
FCC	Face Centered Cubic
FCI	Fuel Cladding Interaction
FCM	Fully Ceramic Micro-Encapsulated
FCT	Fuel Centreline Temperature
FE	Front End
FFRD	Fuel Fragmentation, Relocation, and Dispersal
FGR	Fission Gas Release
FIB	Field Ion Bombardment
FIB	Focused Ion Beam
FIMA	Fissions per Initial Metal Atom
FR	Fuel Rod
FWHM	Full Width Half Maximum
GB	Grain Boundary
GDC	General Design Criteria
GE	General Electric
GNF	Global Nuclear Fuel
GT	Guide Tube
GTRF	Grid-to-Rod Fretting
HAADF	High Angle Annular Dark Field
HANA	High performance Alloy for Nuclear Application
HB	High Burnup
HBS	High Burnup Structure
HBWR	Halden BWR
HDS	Hold-Down Spring
HFIR	High Flux Irradiation Reactor
HGCIM	Half-Gap Channel Interference Metric
HIP	Hot Isostatic Pressing
HPCI	High-Pressure Coolant Injections
HPSC	High Potential Stress Corrosion
HPU	Hydrogen Pick-Up
HPUF	Hydrogen Pick-Up Fraction
HR	Halden Reactor
HRP	Halden Reactor Project
HT	High Temperature
HTGR	High Temperature Gas Reactor
HTP	High Thermal Performance
HWC	Hydrogen Water Chemistry
HWR	Heavy Water Reactor
HZP	Hot Zero Power
IAEA	International Atomic Energy Agency
IASCC	Irradiation Assisted Stress Corrosion Cracking
ICP	Inductively Coupled Plasma
ID	Inner Diameter
INL	Idaho National Laboratory
INNL	Idaho National Nuclear Laboratory
INPO	Institute of Nuclear Power Operations
IRP	Integrated Research Project

Unit conversion

TEMPERATURE		
°C + 273.15 = K	°C × 1.8 + 32 = °F	
T(K)	T(°C)	T(°F)
273	**0**	32
289	16	61
298	25	77
373	**100**	212
473	**200**	392
573	**300**	572
633	360	680
673	**400**	752
773	**500**	932
783	510	950
793	520	968
823	550	1022
833	560	1040
873	**600**	1112
878	605	1121
893	620	1148
923	650	1202
973	**700**	1292
1023	750	1382
1053	780	1436
1073	**800**	1472
1136	863	1585
1143	870	1598
1173	**900**	1652
1273	**1000**	1832
1343	1070	1958
1478	1204	**2200**

Radioactivity	
1 Sv	= 100 Rem
1 Ci	= 3.7×10^{10} Bq = 37 GBq
1 Bq	= 1 s^{-1}

MASS	
kg	lbs
0.454	**1**
1	2.20

DISTANCE	
x (µm)	x (mils)
0.6	0.02
1	0.04
5	0.20
10	0.39
20	0.79
25	0.98
25.4	**1.00**
100	3.94

PRESSURE		
bar	MPa	psi
1	0.1	14
10	**1**	142
70	7	995
70.4	7.04	**1000**
100	10	1421
130	13	1847
155	15.5	2203
704	70.4	**10000**
1000	100	14211

STRESS INTENSITY FACTOR	
MPa√m	ksi√inch
0.91	**1**
1	1.10